



8-1971

Energy Calibration of the Western Michigan University Model en Tandem Accelerator

Michael Joseph Parrott
Western Michigan University

Follow this and additional works at: https://scholarworks.wmich.edu/masters_theses



Part of the Nuclear Commons

Recommended Citation

Parrott, Michael Joseph, "Energy Calibration of the Western Michigan University Model en Tandem Accelerator" (1971). *Masters Theses*. 2910.

https://scholarworks.wmich.edu/masters_theses/2910

This Masters Thesis-Open Access is brought to you for free and open access by the Graduate College at ScholarWorks at WMU. It has been accepted for inclusion in Masters Theses by an authorized administrator of ScholarWorks at WMU. For more information, please contact wmu-scholarworks@wmich.edu.



ENERGY CALIBRATION
OF THE WESTERN MICHIGAN UNIVERSITY
MODEL EN TANDEM ACCELERATOR

by

Michael Joseph Parrott

A Thesis
Submitted to the
Faculty of The Graduate College
in partial fulfillment
of the
Degree of Master of Arts

Western Michigan University
Kalamazoo, Michigan
August 1971

ACKNOWLEDGEMENTS

Special gratitude is expressed to Professor R.E. Shamu and Professor E.M. Bernstein for their guidance and assistance which made this project possible.

Appreciation is also extended to Professor M. Soga for his guidance in the preparing of this manuscript.

Valuable assistance in data taking and analysis was contributed by Mr. M.E. Warren and Mr. S.R. Cooper.

Michael Joseph Parrott

MASTERS THESIS

M-2941

PARROTT, Michael Joseph
ENERGY CALIBRATION OF THE WESTERN MICHIGAN
UNIVERSITY MODEL EN TANDEM ACCELERATOR.

Western Michigan University, M.A., 1971
Physics, nuclear

University Microfilms, A XEROX Company, Ann Arbor, Michigan

THIS DISSERTATION HAS BEEN MICROFILMED EXACTLY AS RECEIVED

Reproduced with permission of the copyright owner. Further reproduction prohibited without permission.

TABLE OF CONTENTS

CHAPTER		PAGE
I	INTRODUCTION	1
II	THEORY	5
	Magnet Constant	5
	Neutron Cross Section Near Threshold	6
	Threshold Frequency Determination	8
	Extrapolation Range	11
III	EXPERIMENTAL	13
	Accelerator	13
	Energy Analyzing System	16
	Neutron Detection	17
	Targets	18
	Procedure	21
IV	RESULTS AND DISCUSSION	26
V	SUMMARY AND CONCLUSIONS	43
	APPENDIX I	46
	APPENDIX II	48
	BIBLIOGRAPHY	58

FIGURES

FIGURES		PAGE
I	Target Illustration	10
II	W.M.U. Accelerator Lab.	15
III	Ice Target Assembly	20
IV	Threshold Measurement of ${}^7\text{Li}(p,n){}^7\text{Be}$	28
V	Threshold Measurement of ${}^{13}\text{C}(p,n){}^{13}\text{N}$	29
VI	Threshold Measurement of ${}^{19}\text{F}(p,n){}^{19}\text{Ne}$	30
VII	Threshold Measurement of ${}^{27}\text{Al}(p,n){}^{27}\text{Si}$	31
VIII	Threshold Measurement of ${}^{12}\text{C}(\alpha,n){}^{15}\text{O}, (2^+)$	32
IX	Threshold Measurement of $\text{D}({}^{16}\text{O},n){}^{17}\text{F}, (4^+)$	33
X	Threshold Measurement of $\text{D}({}^{16}\text{O},n){}^{17}\text{F}, (3^+)$	34
XI	Threshold Measurement of ${}^{12}\text{C}(\alpha,n){}^{15}\text{O}, (1^+)$	35
XII	Threshold Measurement of $\text{D}({}^{16}\text{O},n){}^{17}\text{F}, (2^+)$	36
XIII	Magnet Constant Versus Proton NMR Frequency	38

TABLES

TABLES	PAGE
I Calibration Reaction Summary	22

INTRODUCTION

Tandem accelerators have proven to be very useful instruments for experimental studies of nuclear structure. Many properties of nuclei may be investigated with ease, since a stable beam of charged heavy particles which is very well-defined in energy can be produced. Tandem accelerators which can produce beams of protons with energy ranging from 2 to about 20 MeV are currently in operation, while those that produce protons with energies as high as 40 MeV have been designed. In addition to accelerating protons this type of machine can accelerate heavier particles such as deuterons, helium ions, and oxygen ions with a minimum of effort needed to change from one kind of particle to another. This important advantage is realized because the ion source is external to the accelerating equipment.

The energy of the accelerated beam of particles is determined by passing this beam through an uniform magnetic field. The strength of this field is normally measured at a point by means of a nuclear-magnetic-resonance technique. However, the field at this point may not have the same value as the average field experienced by a particle over its trajectory through the magnet. It is well known, also, that fringing fields affect a particle at the regions where a particle enters and leaves the magnet. For these reasons it is necessary to provide energy calibration for the accelerator analyzing system over the full range of magnet fields possible. This range of fields for the Western Michigan University analyzing magnet, for example, is such that particles with energies from about 2 to 60 MeV equivalent proton

energy may be analyzed.

A common method employed for energy calibrations is the determination of the analyzing magnet field at which neutrons are first emitted from a given reaction. The incident particle energy at which the neutrons are first emitted is called the neutron threshold energy. For a number of different reactions this threshold energy is known from absolute measurements of the incident particle energy at threshold. Marion¹ has reviewed several neutron threshold measurements and has tabulated recommended values for the threshold energies. Below about 6 MeV (p,n) thresholds are easily observable using a simple neutron detector called a long counter. He has listed various useful (p,n) thresholds in this range. Above 6 MeV, though, it is difficult to observe (p,n) thresholds with a long counter because the neutron background becomes large. He has suggested other useful reactions for accelerator calibration at these higher analyzing magnet fields. One such reaction, for example, is the $D(^{16}\text{O},n)^{17}\text{F}$ reaction.

If one reverses the roles of the incident and target particles in the $^{16}\text{O}(d,n)^{17}\text{F}$ reaction, the different charge states of the incident ^{16}O particle in the $D(^{16}\text{O},n)^{17}\text{F}$ reaction provide several higher magnet field calibration points². The incident energy of the ^{16}O ions at threshold may be easily calculated from an absolute measurement by Bondelid et al.³ of the incident deuteron energy in the $^{16}\text{O}(d,n)^{17}\text{F}$ reaction threshold. The ^{16}O ion calibration points are advantageous, since the neutron background from the ^{16}O ions is low, making it possible to perform the measurements using a long counter.

Marion also has listed several (α,n) thresholds as possible

higher magnet field calibration points. Of the (α ,n) reactions listed, the $^{12}\text{C}(\alpha, n)^{15}\text{O}$ reaction has been observed through ^{15}O positron decay by Nelson *et al.*⁴ and Black *et al.*⁵ However, no absolute measurement of the incident alpha energy at threshold has been made. The threshold energy tabulated by Marion for this reaction was calculated from the masses involved. It should be pointed out that, due to the Lewis effect, the "apparent" threshold position and the "true" position calculated from the Q value can differ by 100 to 200 eV¹.

Overly *et al.*⁶, in their calibration of the Yale University HVEC model MP tandem, used a long counter to observe a few of the (p,n) thresholds suggested by Marion in the range below 6 MeV incident proton energy. They noted that neutron and gamma ray background for (p,n) thresholds above 6 MeV made direct neutron observation impossible. For this reason, those (p,n) thresholds which were above 6 MeV had to be observed by delayed counting of decay positrons from short-lived residual nuclei. Further high magnet field calibration points, for this calibration work, were obtained by observing the $\text{D}(^{16}\text{O}, n)^{17}\text{F}$ reaction threshold with a long counter for the 2⁺, 3⁺, 4⁺, and 5⁺ charge states of the ^{16}O ion. It is noted that throughout their measurements, the current of the analyzing magnet had to be recycled by an empirically determined recipe in order to achieve reproducibility.

The purpose of the present work was to provide energy calibration for the Western Michigan University 12 MeV model EN tandem accelerator. The $^7\text{Li}(p, n)^7\text{Be}$, $^{13}\text{C}(p, n)^{13}\text{N}$, $^{19}\text{F}(p, n)^{19}\text{Ne}$, and $^{27}\text{Al}(p, n)^{27}\text{Si}$ thresholds were used as calibration points below 6 MeV. Above 6 MeV equiv-

alent proton energy the 2^+ , 3^+ , and 4^+ charge states of the incident ^{16}O particle in the $\text{D}(^{16}\text{O},\text{n})^{17}\text{F}$ reaction provided neutron threshold calibration points. In addition, the possibility of employing the 1^+ and 2^+ charge states of the alpha particle in the $^{12}\text{C}(\alpha,\text{n})^{15}\text{O}$ and $^{16}\text{O}(\alpha,\text{n})^{19}\text{Ne}$ reactions as neutron threshold calibration points in this higher energy range was investigated.

THEORY

Magnet Constant

The energy of a beam of charged particles, traveling a predetermined path through a magnetic field of a momentum analyzing magnet, is related to the magnetic field by the magnet constant, K . This magnet constant may be defined as follows.

Consider a particle of charge, q , and momentum, p , moving in a plane normal to a uniform, static magnetic field of magnetic induction, B . As shown, e.g., in Jackson⁷, this particle will move in a circular path of radius, r , given by the expression:

$$p = B q r. \quad (1)$$

Thus, for a fixed radius of curvature, r , a measurement of the magnetic induction may be employed to determine the charged particle's momentum. If the rest mass, m , of the particle is known, the particle's kinetic energy, E , can then be found using the expression:

$$p = \sqrt{2mE + E^2/c^2}, \quad (2)$$

where p is the relativistic momentum of the particle and c is the speed of light. Squaring both sides of Eq. (1) and using Eq. (2), one obtains:

$$B^2 = \left(1/q^2 r^2\right) \left(2mE + E^2/c^2\right). \quad (3)$$

The magnetic field is usually measured by a nuclear-magnetic-resonance (NMR) technique and may be written:

$$B = K' f, \quad (4)$$

where K' is a constant and f is the resonance frequency. Substituting

Eq. (4) into Eq. (3), one gets:

$$(K'f)^2 = \left(2mc^2E/r^2g^2c^2 \right) \left(1 + E/2mc^2 \right). \quad (5)$$

Expressing E and mc^2 in keV, writing q^2 as Q^2e^2 , and combining constants so that the magnet constant, $K=(K')^2r^2c^2/2$, one obtains:

$$K = \left(mE/Q^2f^2 \right) \left(1 + E/2mc^2 \right). \quad (6)$$

If m is expressed in unified mass units (u) and f in megahertz (MHz), the units of K are u-keV/MHz².

Once the magnet constant has been determined, Eq. (6) can be solved easily for E to calculate the energy of an incident particle corresponding to a specific NMR frequency on the field monitoring equipment. One obtains as the expression for E:

$$E = -mc^2 + \sqrt{(mc^2)^2 + 2(KQ^2mc^2f^2)/m}. \quad (7)$$

Neutron Cross Section Near Threshold

A value of K may be determined by observing a neutron threshold for a particular endothermic reaction. The NMR frequency at which the threshold takes place corresponds to the threshold energy for the emission of neutrons from that reaction. The usefulness of this method arises from the behavior of the total neutron emission cross section, i.e., the cross section integrated over all angles, near threshold. The cross section versus energy curve for S-wave neutrons has infinite slope at threshold⁸. Thus, a very sharp rise in neutron yield may be observed. A number of neutron threshold energies have been measured and calculated¹. These served as the energy values used to determine K in this experiment.

The energy dependence of the neutron emission cross section

immediately above threshold can be determined as follows. Consider the endothermic reaction $A+a \rightarrow B+b$. The number of transitions per unit time, w , is given by the Golden Rule for constant transitions, discussed, e.g., by Merzbacher⁹:

$$w = \frac{2\pi}{\hbar} |\mathcal{H}|^2 \frac{dn}{dE}, \quad (8)$$

where \mathcal{H} is the matrix element of the perturbation causing the transition, and dn/dE is the energy density of final states. Since S-wave neutrons are emitted isotropically in the center-of-mass system, it can be shown that the number of states available to a neutron in a volume, V , with momentum between p_n and p_n+dp_n , is given by:

$$dn = \frac{4\pi p_n^2 dp_n V}{(2\pi\hbar)^3}. \quad (9)$$

Also one may write:

$$dE = v_n dp_n \quad (10)$$

where v_n is the velocity of the neutron, so that:

$$\frac{dn}{dE} \propto \frac{p_n^2}{v_n} \propto v_n. \quad (11)$$

The matrix element $|\mathcal{H}|$ can be written¹⁰:

$$|\mathcal{H}| = \bar{U} \times \text{Volume of nucleus} \times \overline{|\Psi_{\text{initial}} \Psi_{\text{final}}|}, \quad (12)$$

where $\overline{|\Psi_i \Psi_f|}$ is a suitable average of the product of the initial and final state wave functions over the volume of the nucleus and \bar{U} is the average interaction energy. Thus, one may write:

$$|\mathcal{H}|^2 \propto (\bar{U} \times \text{Volume of nucleus})^2 \times \exp(-G_a), \quad (13)$$

where $\exp(-G_a)$ is a coulomb barrier term, since "a" is a charged particle. The definition of the cross section, σ , is essentially contained in the relation:

$$\begin{aligned} \text{Nos. of transitions/sec} \\ \text{per "A" nucleus} \end{aligned} = n_a \times v_{\text{"a" relative "A" to}} \times \sigma \quad (14)$$

where n_a is the density of the incident particles. For massive "A", the velocity of "a" relative to "A" in Eq. (14) can be written as v_a , the velocity of "a" in the center-of-mass frame. Thus the cross section can be expressed:

$$\sigma \propto v_n/v_a \exp(-G_a). \quad (15)$$

Immediately above threshold, the energy of the emitted neutron is small ($v_n \ll v_a$), such that v_a is essentially constant. Also, since $\exp(-G_a)$ depends on the energy of the incoming particle, $\exp(-G_a)$ is essentially constant. Therefore, the cross section is proportional to the velocity of the emitted neutron, which is proportional to the square root of the difference between the threshold energy, E_{TH} , and incident particle energy within the target, E :

$$\sigma \propto v_n \propto (E - E_{TH})^{1/2}. \quad (16)$$

Threshold Frequency Determination

Consider a monoenergetic beam of N charged particles having a kinetic energy, E_a , incident normal to a thick target with a density of n nuclei per cm^3 (See Fig. I.). Assume that E_a is just above the threshold energy, E_{TH} , so that the specific energy loss, dE/dx ¹¹, of the charged particles in the target is essentially constant over the energy range E_a to E_{TH} . Let Δx be the distance from the point where the particle energy has been reduced to the minimum energy for neutron production, i.e., E_{TH} , to the surface of the target (We ignore here energy straggling.). Consider a target element in Δx of thickness dx , which is a distance x from the plane where the particle energy is E_{TH} (See Fig. I.). Let E be the particle energy within the ele-

Figure I. Illustration of the target parameters used to derive the dependence of neutron yield on incident particle energy.

①

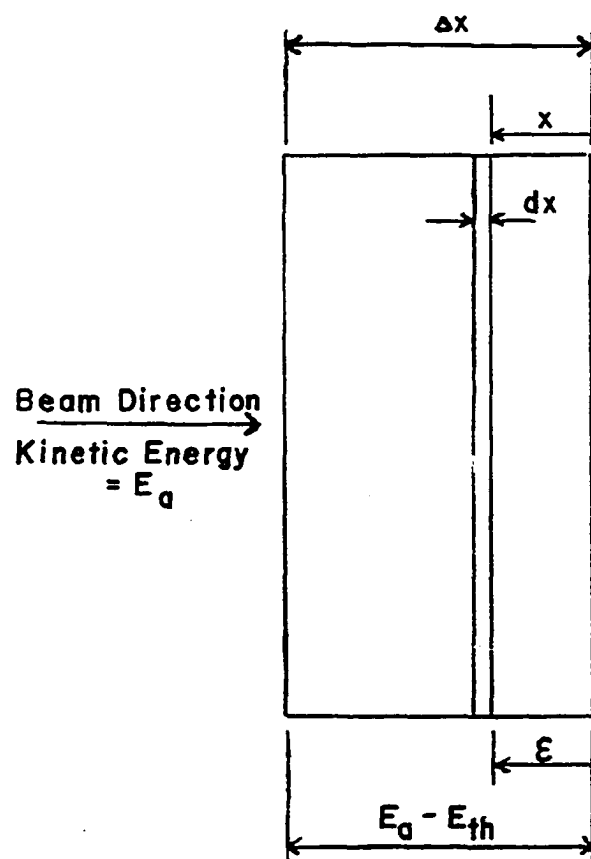


Figure I. TARGET ILLUSTRATION

ment dx . Then one may write:

$$E = E_{TH} + dE/dx \times x \quad (17)$$

or

$$\mathcal{E} = \frac{dE}{dx} \times x, \quad (18)$$

where we have defined $\mathcal{E} = E - E_{TH}$. The yield from the element dx of the target may be written:

$$dY(\mathcal{E}) = N_n \sigma(\mathcal{E}) dx, \quad (19)$$

where $\sigma(\mathcal{E})$ is the neutron emission cross section. In the previous section, Eq. (16), the neutron cross section was shown to be proportional to the square root of :

$$\sigma(\mathcal{E}) \propto (\mathcal{E} - E_{TH})^{1/2} = \mathcal{E}^{1/2} \quad (20)$$

Thus the integrated yield from the target is given by:

$$\int_0^{Y(\mathcal{E}_{max})} dY(\mathcal{E}) \propto \int_0^{\mathcal{E}_a - E_{TH}} \mathcal{E}^{1/2} d\mathcal{E} \propto (\mathcal{E}_a - E_{TH})^{3/2} = \Delta\mathcal{E}^{3/2} \quad (21)$$

where we have used Eq. (19) and Eq. (20) and defined $\Delta\mathcal{E} = \mathcal{E}_a - E_{TH}$.

The threshold energy can be determined by a straight line extrapolation of a plot of net yield, above any background, raised to the 2/3 power versus energy to the energy intercept. In this case, for a small frequency range, a least squares straight line fit (See Appendix I.) of net yield raised to the 2/3 power versus proton NMK frequency extrapolated to the frequency intercept yields the threshold frequency.

Extrapolation Range

As is seen one must be careful to ensure that all the neutrons are being counted, since it is the total yield referred to in Eq. (21). It is shown by Hanson¹², for endothermic reactions, that outgoing

neutrons in the laboratory system are confined to a cone in the forward direction whose half-angle, ψ , is given by:

$$\psi = \sin^{-1} \left[(M_A M_B / M_a M_n) (E - E_{TH}) / E \right]^{1/2} \quad (22)$$

where $E - E_{TH}$ is the extrapolation range and M_A , M_B , M_a , and M_n are the masses in the reaction $A + a \rightarrow B + n$. Thus, for a given half-angle subtended by the neutron detector, there is an extrapolation range, $E - E_{TH}$, for which all the neutrons are counted.

Also, if the targets used are thin, one must be sure to take an extrapolation range which does not extend beyond the target. This ensures that particles which pass through the target have lost sufficient energy that they emerge with an energy less than the threshold energy.

One must also ensure that too many neutrons are not counted. This would happen if there is a resonance near threshold and the extrapolation range included the resonance. For example, in the case of the ${}^7\text{Li}(p,n){}^7\text{Be}$ threshold, the extrapolation range must be taken small enough to exclude the resonance just above threshold.

EXPERIMENTAL

Accelerator

The floor plan of the Western Michigan University tandem accelerator laboratory is shown in Fig. II. The accelerator system consists of a negative ion source, beam accelerating equipment, and an energy analyzing system. The accelerator is a 12 MeV model EN tandem Van de Graaff accelerator manufactured by High Voltage Engineering Corporation.

A general physical description of the accelerator system, as illustrated in Fig. II, follows most easily from a discussion of the principles of operation. Consider, for example, the acceleration of protons. In the ion source neutral hydrogen atoms are ionized to form positive hydrogen ions. After these positive ions have been slightly accelerated, electrons are added to the positive hydrogen ions and a negative hydrogen ion beam, H^- , is produced. The negative ions are then accelerated toward a high voltage terminal at positive potential in the center of the model EN accelerator, which is capable of maintaining a voltage up to 6 million volts. At this point the beam passes through a stripper gas and each H^- ion is stripped of its electrons. The resulting positive ions, protons, are then repelled by the terminal to a maximum energy of 12 MeV. This particular type of machine is also capable of accelerating any heavier positive ions to which a sufficient number of electrons may be added to form a negative beam for the first stage of acceleration, i.e.,

Figure II. W.M.U. Accelerator Lab. The general floor plan of the Western Michigan University tandem accelerator laboratory is shown. The major components of the accelerator system are labeled. The accelerator itself is a model EN 12 MeV tandem Van de Graaff accelerator.

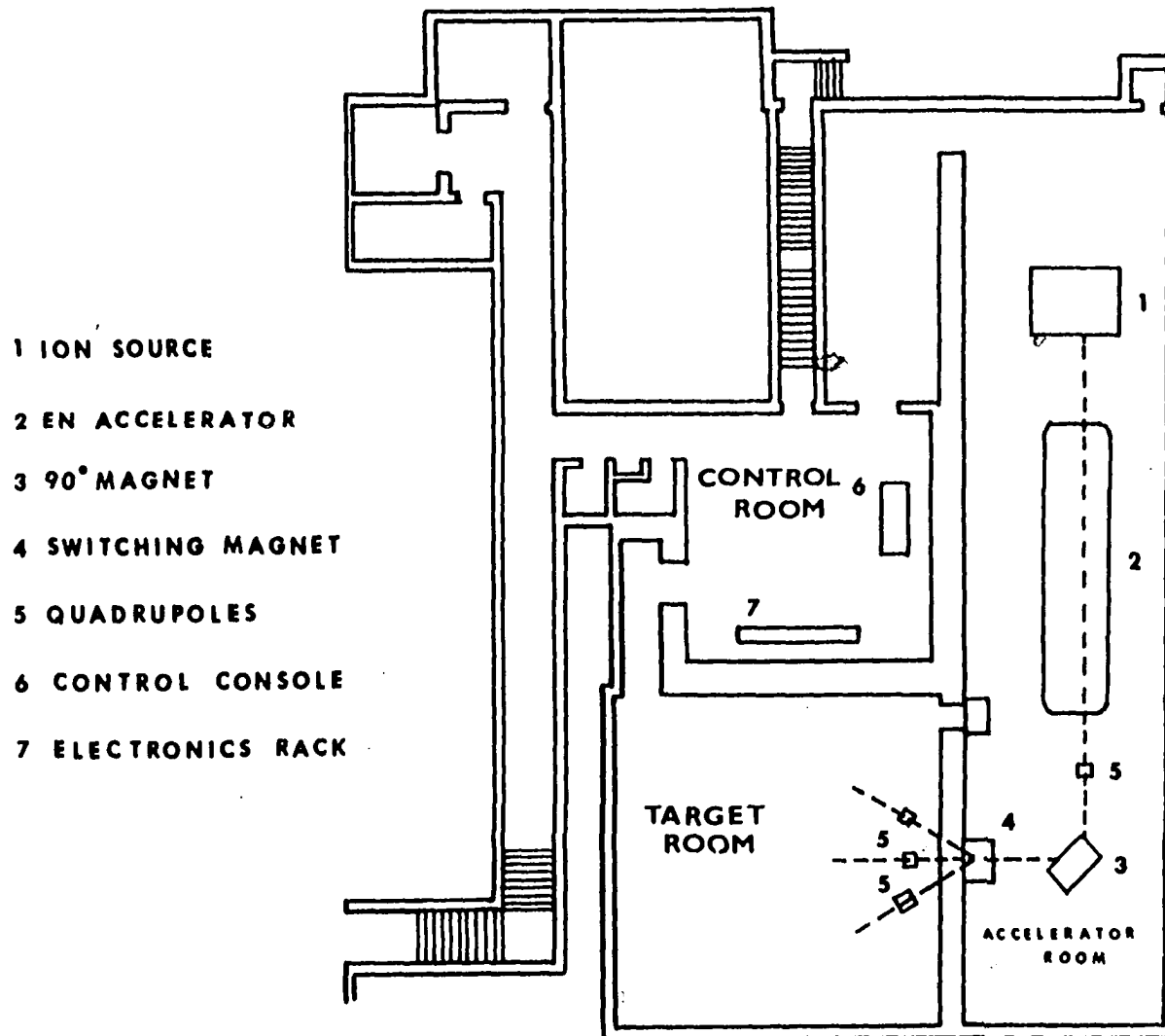


Figure II. W.M.U. ACCELERATOR LAB.

deuterons, helium, and oxygen.

Energy Analyzing System

The accelerated ions pass through a quadrupole magnet and are focused on the object slits of a 90° momentum analyzing magnet. The positive ions of selected mass, charge, and energy will make the 90° turn through the magnet to be focused on the image slits. Through a slit control system, these slits sense any energy imbalance, due to effects such as wandering of the terminal voltage, and cause proper adjustment of the terminal voltage until balance is regained. If, for example, the chosen incident particle begins to deviate from the desired energy to a different energy, the radius of curvature of the particle's path through the magnet changes and the particle strikes one slit. This causes a current imbalance with more current on this slit. The current difference between the two slits is fed back causing proper terminal voltage compensation to maintain balance. Control can also be maintained through a generating voltmeter control system if, for example, the beam is too small to operate the slit control system. Data throughout these measurements were taken with the machine on slit control. The energy analyzed beam passes through a switching magnet to any one of three target room beam lines and focuses via another quadrupole magnet onto the selected target.

The field within the analyzing magnet is determined by a nuclear-magnetic-resonance (NMR) technique. A proton NMR probe is placed at a fixed position within the magnet near its midpoint and close to the beam trajectory. The proton NMR frequency, which is proportional to

the magnetic field, is read directly on a frequency meter. The neutron thresholds measured were such that nearly the full range of analyzing magnet field was investigated.

The components of the beam handling system were manufactured and supplied by Varian, Associates. The analyzing magnet is a double-focusing model 1058 analyzing magnet. This magnet produces a homogeneous field, such that changes in the magnet constant attributable to field homogeneity are less than 1 part in 10^4 . The image and object slits, which define the beam trajectory through the analyzing magnet, are model 9030 adjustable single slits and model 9010 adjustable double slits respectively. Both of these sets of slits are adjustable to within 0.001 inches. The switching magnet and the quadrupole magnets are a model 1035 switching magnet and model 1050 quadrupole doublets respectively. The analyzing magnet field measuring instrument is a model 5002 NMR gaussmeter.

Neutron Detection

A standard long counter was used to detect the neutrons in all of the threshold measurements. The long counter was essentially the same construction as that of Hanson and McKibben¹³, except that an 8 inch diameter polyethelene cylinder was used as the moderator, instead of paraffin. A high voltage of 1500 volts was supplied across the Nancy Wood model G-5-9 BF_3 tube by an Ortec model 446 high voltage power supply. The neutron pulses were preamplified by a model 100C Tennelec low noise preamplifier and then amplified by an Ortec model 485 amplifier. The resulting pulses, approximately 7 volts high,

were recorded by an Ortec model 484 biased scaler.

Targets

Two types of targets were employed for the threshold measurements, solid targets and ice targets. For both cases a target assembly was designed to facilitate the measurement of the thresholds involved.

The solid target assembly consisted of a 3" long, 9/16" O.D., thin-walled stainless steel tube closed at one end by a 0.025"-thick stainless steel cap. A 3/16"-thick, 2" O.D. flange at the other end joined onto the target room beam line. The assembly was electrically insulated from the beam line by a 3/16"-thick lucite spacer and by using nylon bolts. The solid targets are held perpendicular to the beam path at the closed end of the 3" tube by a circular clip which fits snugly to the inner diameter of the tube. This assembly was employed for all the measurements except the $D(^{16}\text{O},n)^{17}\text{F}$ measurements.

Figure III shows the target assembly designed to make frozen D_2O ice targets for the $D(^{16}\text{O},n)^{17}\text{F}$ measurements. The 8" liquid nitrogen reservoir was filled with approximately 1" of liquid nitrogen and a measured amount of heavy water was bled into the system through the Cu tubing at the bottom of the assembly. The reservoir was then filled with liquid nitrogen and the beam allowed to hit the ice target. During a normal run, the liquid nitrogen lasted at least 30 minutes. The amount of heavy water frozen on the target assembly was controlled by letting a reservoir of heavy water come into equilibrium with a fixed volume through a manifold. The opening to the res-

Figure III. Ice Target Assembly. The assembly designed for the making of frozen D_2O ice targets for the $D(^{16}O, n)^{17}F$ threshold measurements is shown.

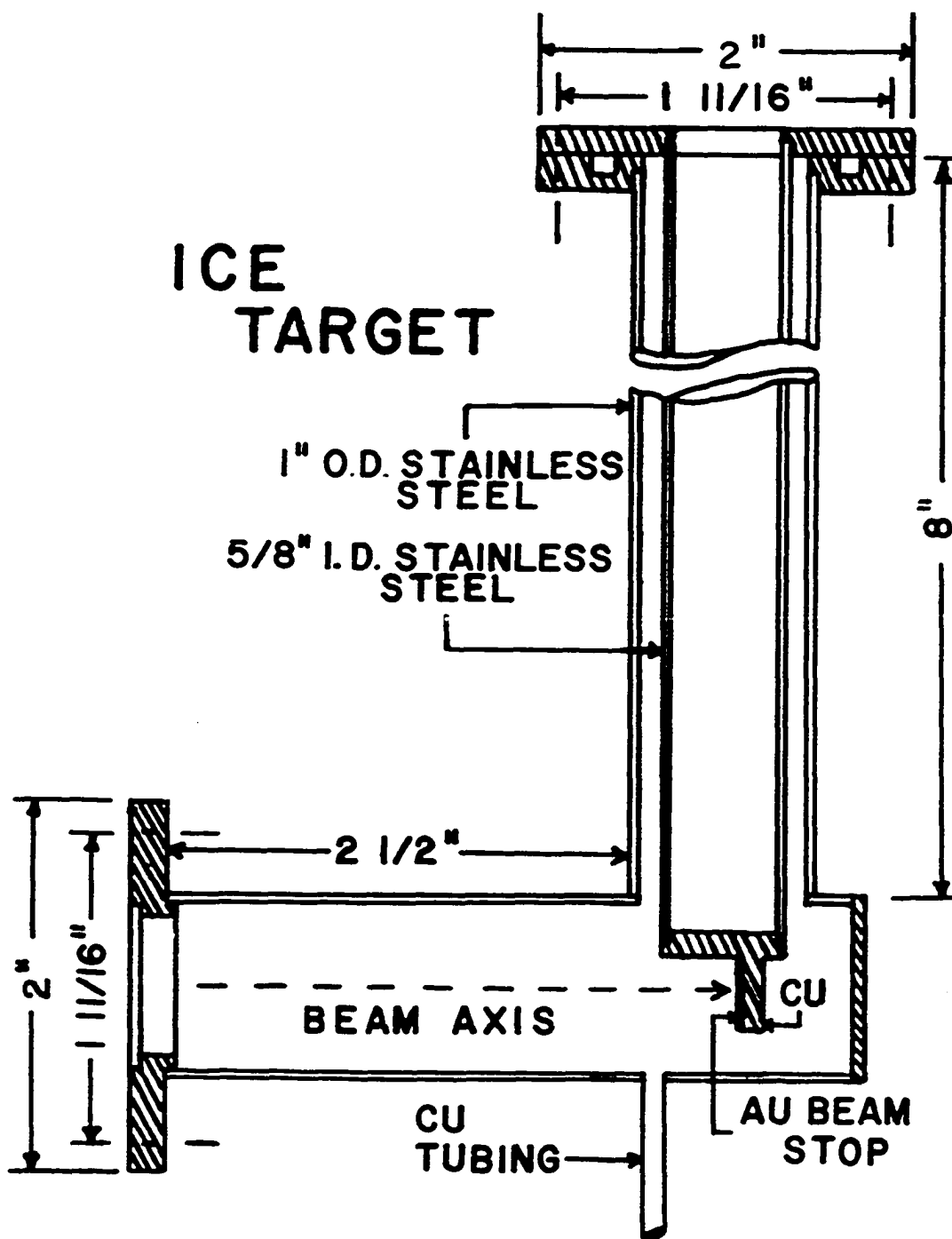


Figure III. ICE TARGET ASSEMBLY

ervoir was then shut and the vapor bled through a needle valve to the cold target backing. For the thresholds other than $D(^{16}\text{O},n)^{17}\text{F}$, the individual targets are listed in Table I. The thick LiF and CaF_2 crystals were supplied by Harschaw, while the $100 \mu\text{g}/\text{cm}^2$ carbon foil was supplied by Yisum Reasearch Development Co. and the ^{13}C foil obtained from Argonne National Lab. All of the thin foils were mounted on gold or tantalum backings.

A 3/16"-diameter tantalum or gold collimator, located about 15" in front of the target position, served to define the beam spot on the targets. In addition, a 3/8"-diameter tantalum anti-scattering baffle was mounted on the flange of each target assembly to prevent charged particles scattered by the collimator from striking stainless steel.

^o Procedure

Analyzing magnet differential hysteresis may affect the relationship between the field measured at the probe position and the average field sampled by a beam particle. To reduce such effects, a pre-determined recipe of recycling the magnet, suggested by Varian, Associates, was utilized. The magnet current was reduced to zero for two minutes. The magnet was then brought to maximum field for another two minutes and then down to the desired field. It is noted that this procedure is exactly opposite that of Overly *et al.*⁶ Before each measurement the image and object slits were set and the magnet recycled to a point sufficiently below threshold so that the linearly varying background could be determined. The magnet field was increased

TABLE I
 CALIBRATION REACTIONS

REACTION	TARGET	EXTR. RANGE (keV)	SLIT WIDTH (inches)		INDIVIDUAL THRESH. (MHz)	FREQ.	THRESHOLD ENERGY (keV)	MAGNET CONSTANT ($\mu\text{-keV}/\text{MHz}^2$)
${}^7\text{Li}(p,n){}^7\text{Be}$	LiF	2.5	0.0100	0.0050	12.71480	± 0.00019	1880.6 \pm 0.07	11.72744 \pm 0.0016*
			0.0100	0.0050	12.71526	± 0.00019		
			0.0100	0.0050	12.71663	± 0.00041		
			0.0150	0.0100	12.71569	± 0.00014		
			0.0150	0.0100	12.71489	± 0.00017		
			0.0150	0.0100	12.71662	± 0.00034		
			FREQ. RESULT =			12.71565		
${}^{13}\text{C}(p,n){}^{13}\text{N}$	${}^{13}\text{C}$ foil	3	0.0150	0.0100	16.68384	± 0.00007	3235.7 \pm 0.7	11.72774 \pm 0.0039*
			0.0150	0.0100	16.68344	± 0.00008		
			0.0150	0.0100	16.68251	± 0.00005		
			0.0100	0.0050	16.68736	± 0.00007		
			0.0150	0.0100	16.68767	± 0.00023		
			0.0150	0.0100	16.68502	± 0.00034		
			FREQ. RESULT =			16.68497		
${}^{19}\text{F}(p,n){}^{19}\text{Ne}$	CaF ₂	9	0.0100	0.0050	19.0971	± 0.00205	4234.3 \pm 0.8	11.72462 \pm 0.0036*
			0.0100	0.0050	19.0941	± 0.00239		
			0.0100	0.0050	19.0942	± 0.00321		
			FREQ. RESULT =			19.0955		

TABLE I (cont.)
 CALIBRATION REACTIONS

REACTION	TARGET	EXTR. RANGE (keV)	SLIT WIDTH OBJ. (inches)	IM. (inches)	INDIVIDUAL THRESH. FREQ. (MHz)	THRESHOLD ENERGY (keV)	MAGNET CONSTANT (μ -keV/MHz ²)
$^{27}\text{Al}(p,n)^{27}\text{Si}$	Thick Al foil	7	0.0050	0.0050	22.37181 ± 0.00026	5796.9 ± 3.8	11.70475 ± 0.0081
			0.0050	0.0050	22.36848 ± 0.00022	5794.5 ± 2.4^a	11.69989 ± 0.0055
			0.0050	0.0050	22.36784 ± 0.00021	5802.9 ± 3.8^b	$11.71690 \pm 0.0081^*$
			0.0050	0.0050	22.37315 ± 0.00030		
			0.0100	0.0050	22.36746 ± 0.00027		
			FREQ. RESULT = 22.36974 ± 0.0026				
$^{12}\text{C}(\alpha,n)^{15}\text{O}$ (2^+)	100 g/cm ² C foil	40	0.0150	0.0100	31.14462 ± 0.0015	11346.3 ± 1.7^c	11.71948 ± 0.0020
			0.0150	0.0100	31.14488 ± 0.0019	11340.3 ± 1.0^d	11.71328 ± 0.0014
					FREQ. RESULT = 31.14475 ± 0.0012		11343.4 ± 5.7^e
$\text{D}(^{16}\text{O},n)^{17}\text{F}$ (4^+)	D ₂ O ice	200	0.0150	0.0100	35.20154 ± 0.0023	14525.0 ± 5	$11.71689 \pm 0.0086^*$
			0.0150	0.0100	35.21731 ± 0.0033		
					FREQ. RESULT = 35.20943 ± 0.0113		
$\text{D}(^{16}\text{O},n)^{17}\text{F}$ (3^+)	D ₂ O ice	150	0.0150	0.0100	46.97189 ± 0.0055	14525.5 ± 5	$11.71193 \pm 0.0110^*$
			0.0150	0.0100	46.94302 ± 0.0043		
					FREQ. RESULT = 46.95746 ± 0.0207		

TABLE I (cont.)
 CALIBRATION REACTIONS

REACTION	TARGET	EXTR. RANGE (keV)	SLIT WIDTH OBJ. IM. (inches)	INDIVIDUAL THRESH. (MHz)	FREQ.	THRESHOLD ENERGY (keV)	MAGNET CONSTANT (u-keV/MHz ²)
$^{12}\text{C}(\alpha, n)^{15}\text{O}$ (1 ⁺)	100 g/cm ² C foil	40	0.0150	0.0100	62.32333 ± 0.00495	11346.3 ± 1.7 ^c	11.70193 ± 0.0063
			0.0150	0.0100	62.35488 ± 0.00370	11340.3 ± 1.0 ^d	11.65974 ± 0.0061
			0.0150	0.0100	62.34314 ± 0.00410	11343.4 ± 5.7 ^e	11.69894 ± 0.0084*
			FREQ. RESULT = 62.34046 ± 0.0161				
$\text{D}(^{16}\text{O}, n)^{17}\text{F}$ (2 ⁺)	D ₂ O ice	100	0.0150	0.0100	70.50348 ± 0.0070	14526.0 ± 5	11.69418 ± 0.0070*
			0.0150	0.0100	70.48058 ± 0.0087		
			FREQ. RESULT = 70.49203 ± 0.0171				

* Points used for Fig. XIII.

- a) Bonner et al., energy value.
- b) Freeman et al., energy value.
- c) Calculated with Mattauch et al., ¹⁵O mass.
- d) Calculated with Hensley ¹⁵O mass.
- e) Calculated with average ¹⁵O mass.

in small convenient increments and neutrons counted for equal intervals, determined by a Brookhaven Instruments' model 1000 current integrator along with an Ortec model 431 timer-scaler.

For the case when the ice target assembly was used, measurements were made with nitrogen only in the target assembly and with no nitrogen or ice and no increase in neutron yield due to carbon build-up was observed.

The total slit width for the image and object slits for each threshold measurement is listed in Table I.

Care was taken to ensure that points included in the extrapolation range of the $2/3$ power plots represented the total yield of neutrons as discussed in the Theory section.

RESULTS AND DISCUSSION

The results of the individual threshold measurements are listed in Table I. Included in this table are the targets, extrapolation ranges, the image and object slit widths, and the threshold energy values used. Typical threshold data is presented in Figures IV-XII. Two plots are shown on these figures. The top plot is the yield versus proton NMR frequency, with a line shown for the linearly varying background where it differs significantly from zero. The bottom plot is net yield to the $2/3$ power versus proton NMR frequency showing the least squares straight line fit (See Appendix I.) of the points above threshold. The point where the straight line fit intercepts the zero line of the net yield to the $2/3$ power is the threshold frequency. The intercept for all the measurements is listed in Table I. In the case where no error bars are shown for the points on these figures, the error is about the same size or smaller than the size of the point. Figure XIII shows the results of the K versus f curve (See Theory section for the derivation of the magnet constant, K.). The nine neutron thresholds measured represent points covering almost the entire range of analyzing magnet field.

In addition an unsuccessful attempt was made to observe the the $^{16}\text{O}(\alpha, n)^{19}\text{Ne}$ threshold for two more points at higher magnet fields. No increase in neutron yield was observed near the expected threshold frequency, although a rise in neutron yield was observed almost 300 keV above this point. This effect is unexplained.

Figures IV-XII. Threshold Measurements. Typical data taken for each of the nine thresholds measured is displayed. The figures consist of two plots. The upper plot is a plot of neutron yield versus proton NMR frequency, with a horizontal line representing the average background below threshold, where the background differs significantly from zero. The lower plot is a plot of net yield above background to the $2/3$ power for points above threshold versus proton NMR frequency. A least squares straight line fit, as discussed in Appendix I, is shown. The intercept of the straight line fit with the zero of net yield to the $2/3$ power is the threshold frequency. In all cases where error bars are not shown, the error is about the same size or smaller than the point itself.

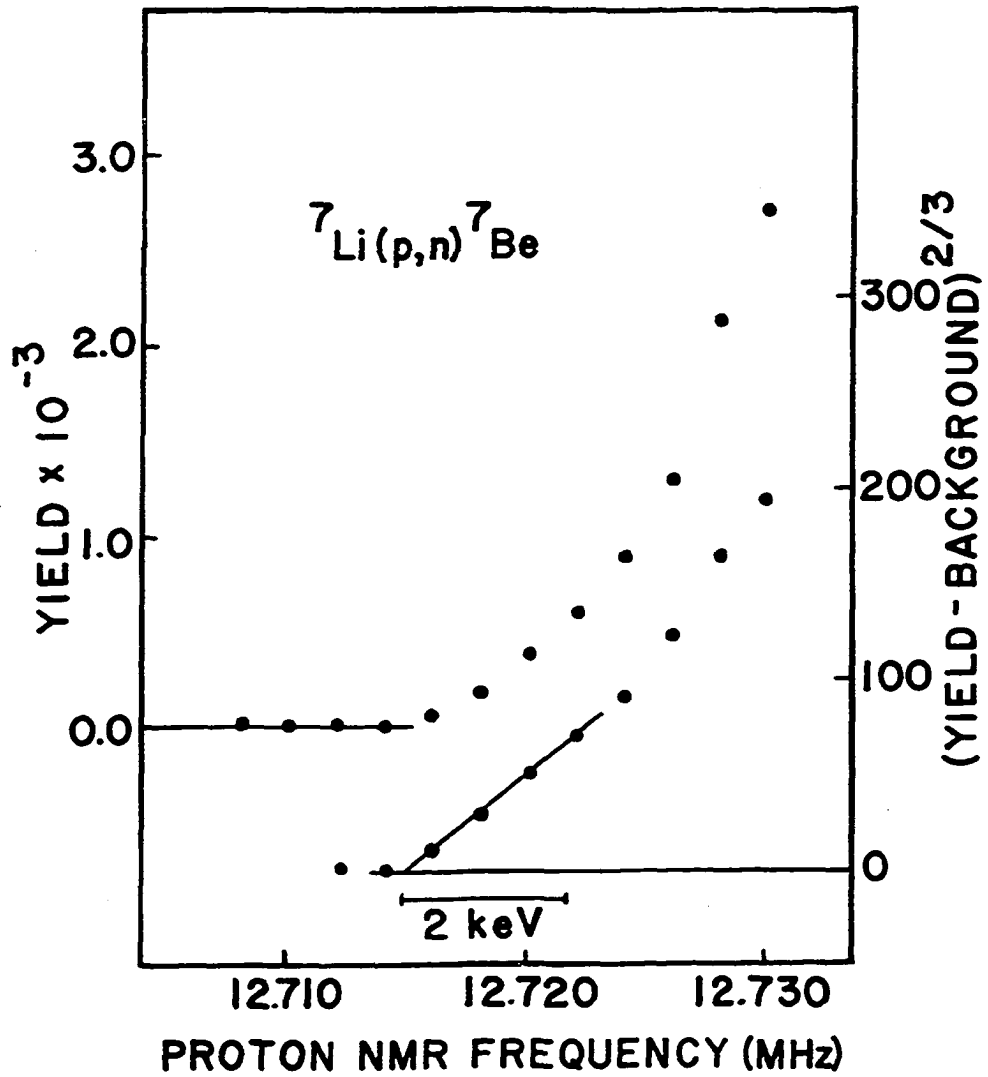


Figure IV. THRESHOLD MEASUREMENTS

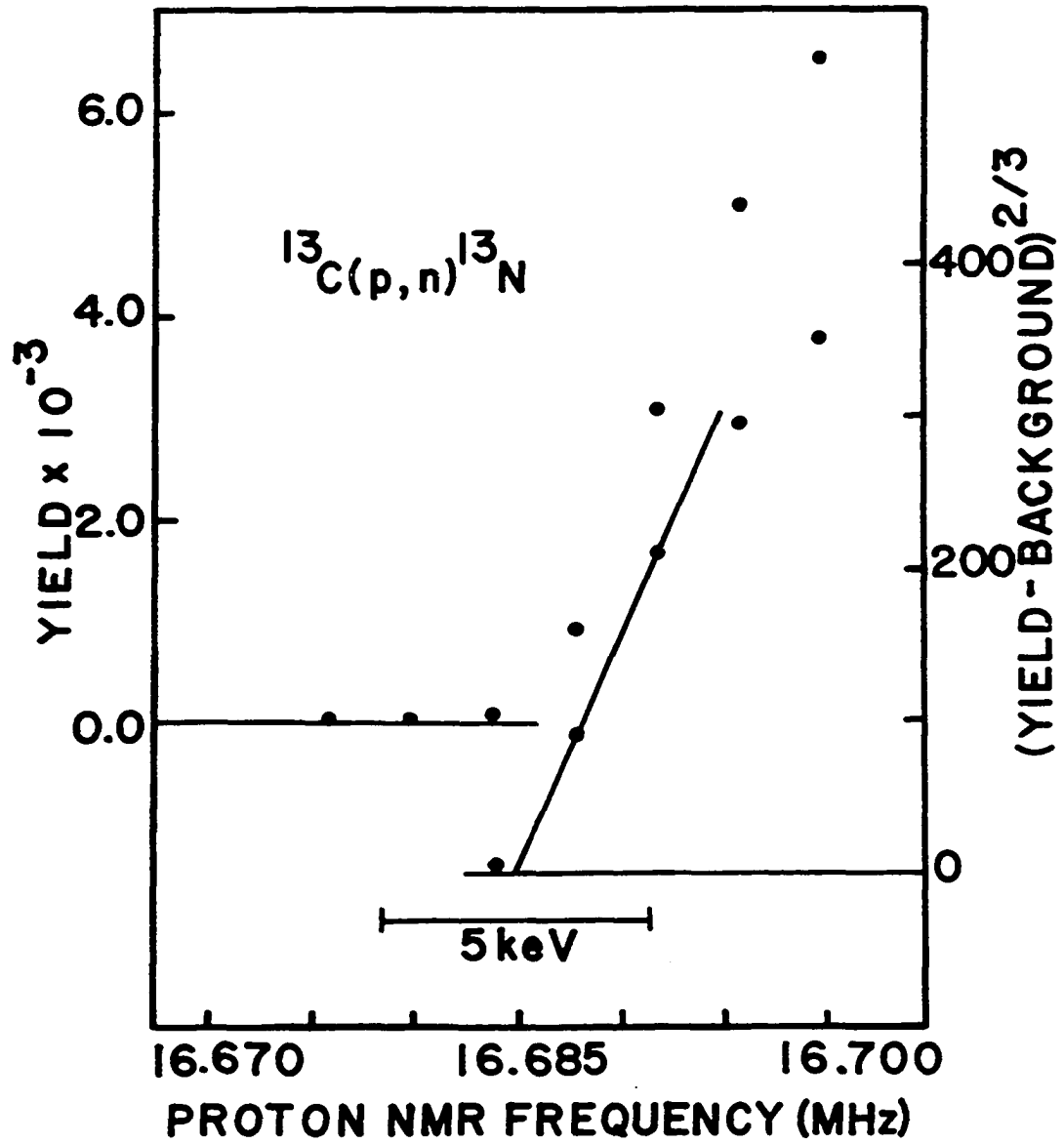


Figure V. THRESHOLD MEASUREMENTS

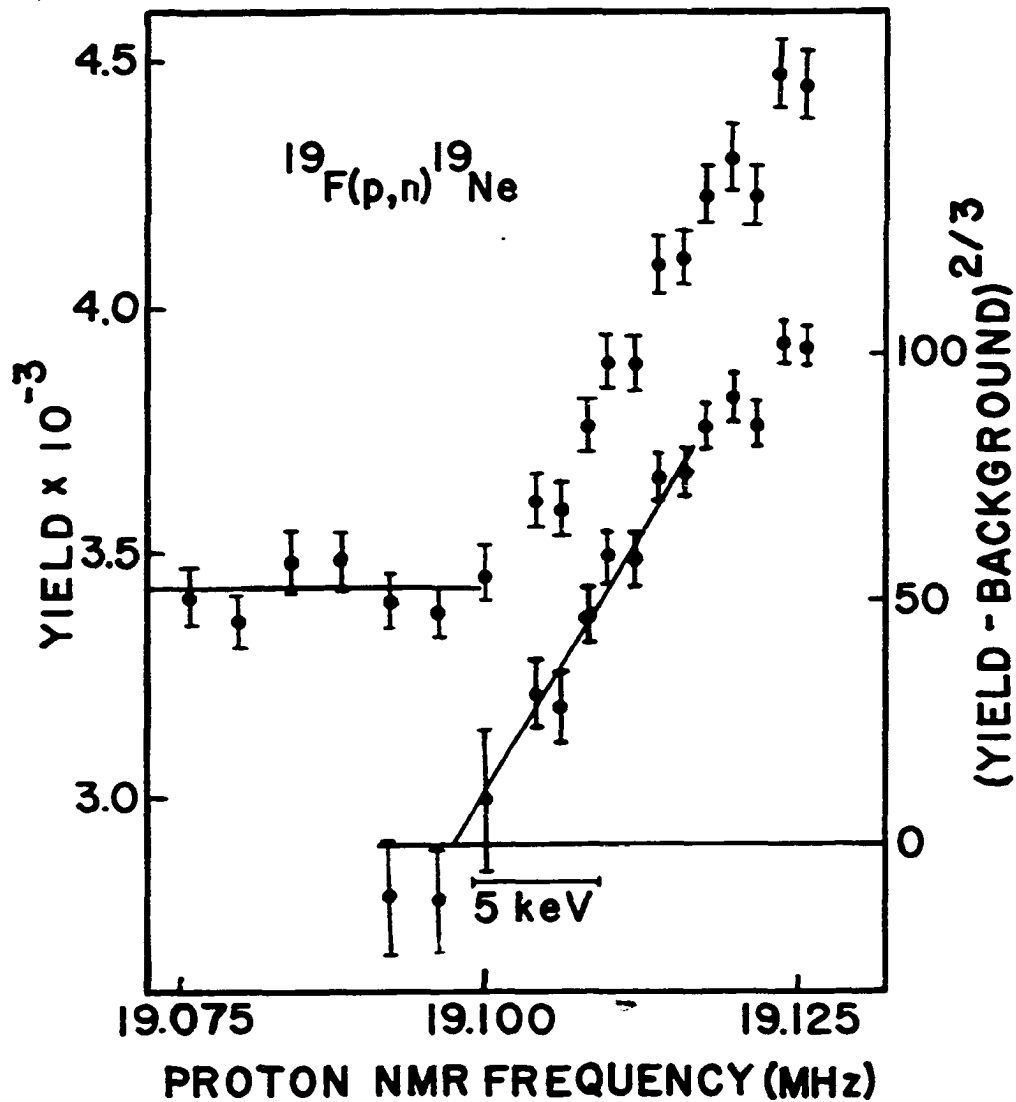


Figure VI. THRESHOLD MEASUREMENTS

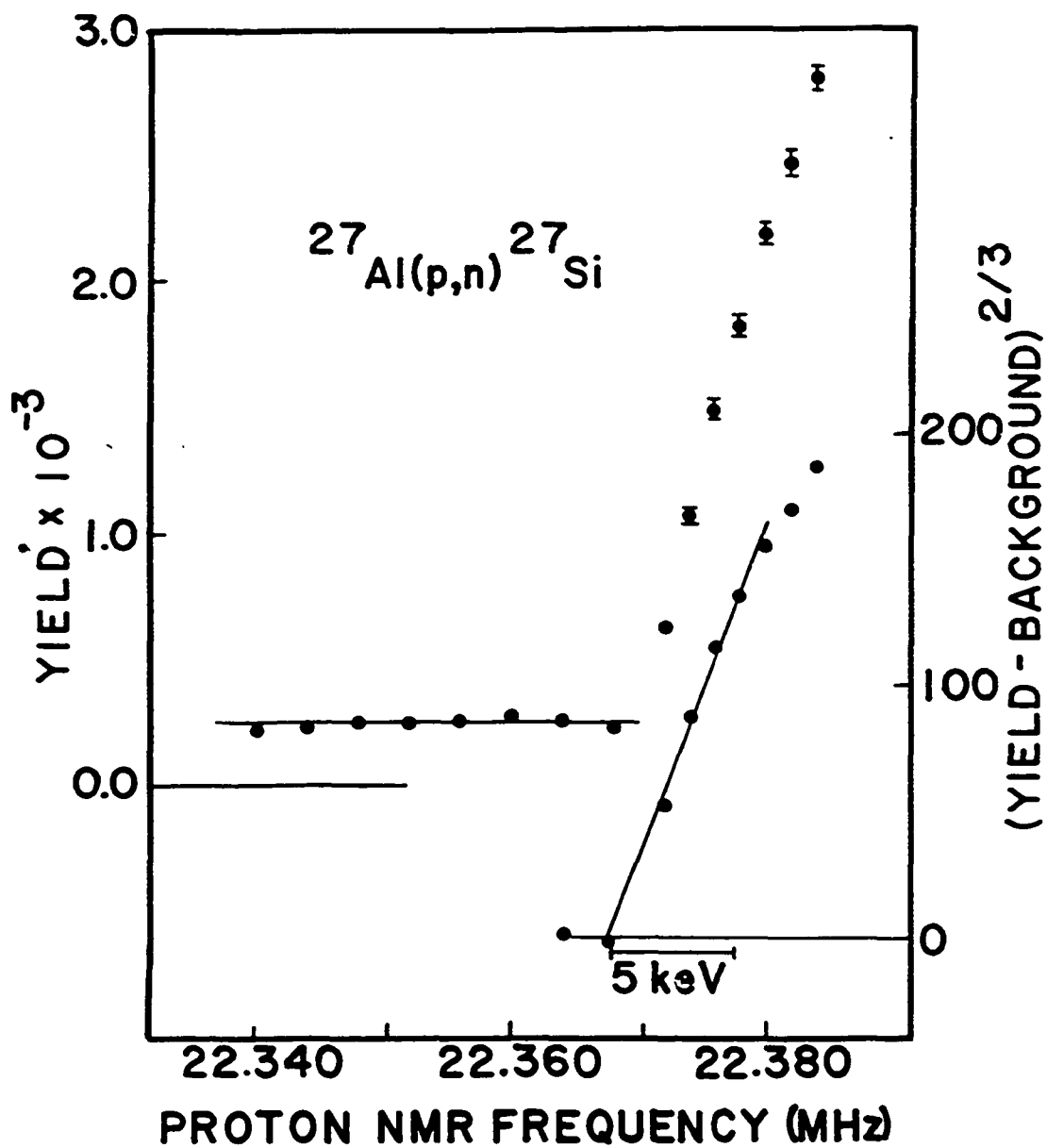


Figure VII. THRESHOLD MEASUREMENTS

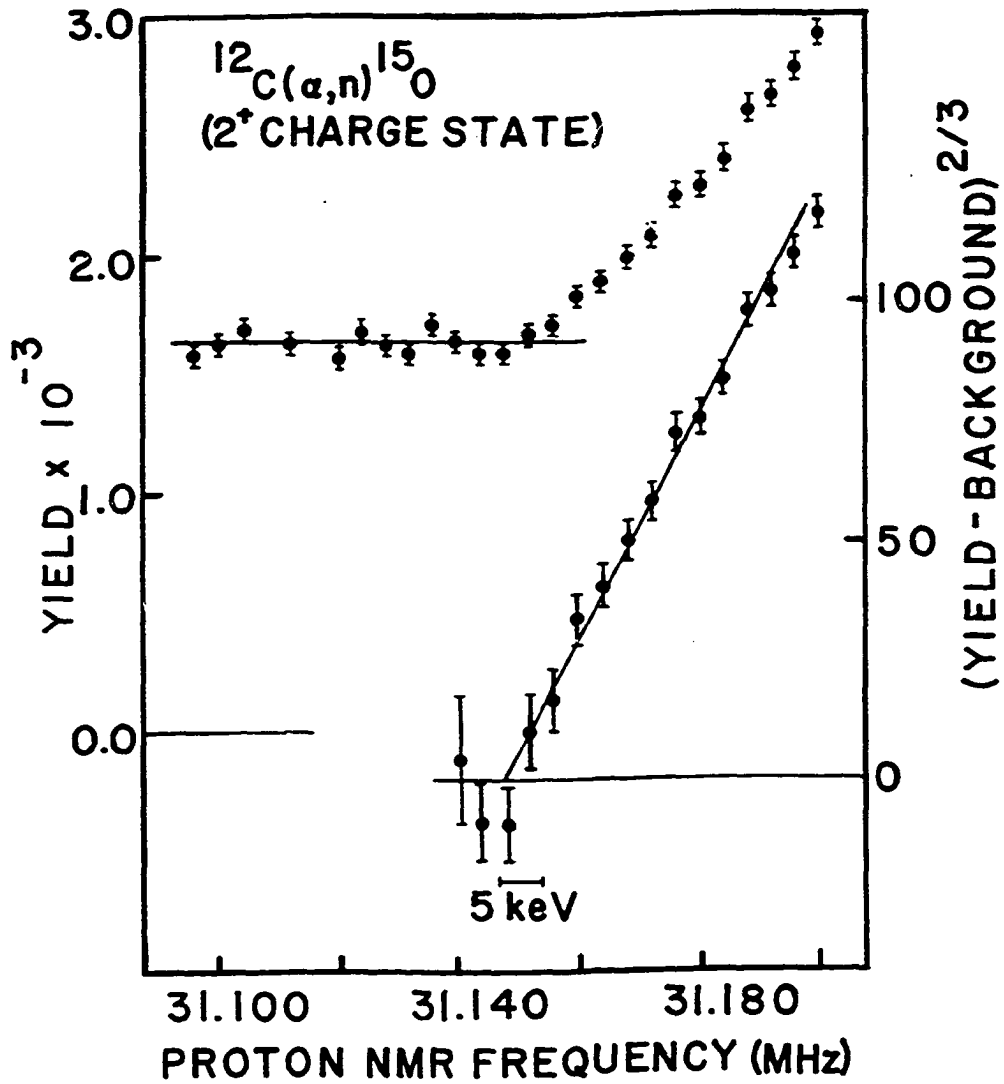


Figure VIII. THRESHOLD MEASUREMENTS

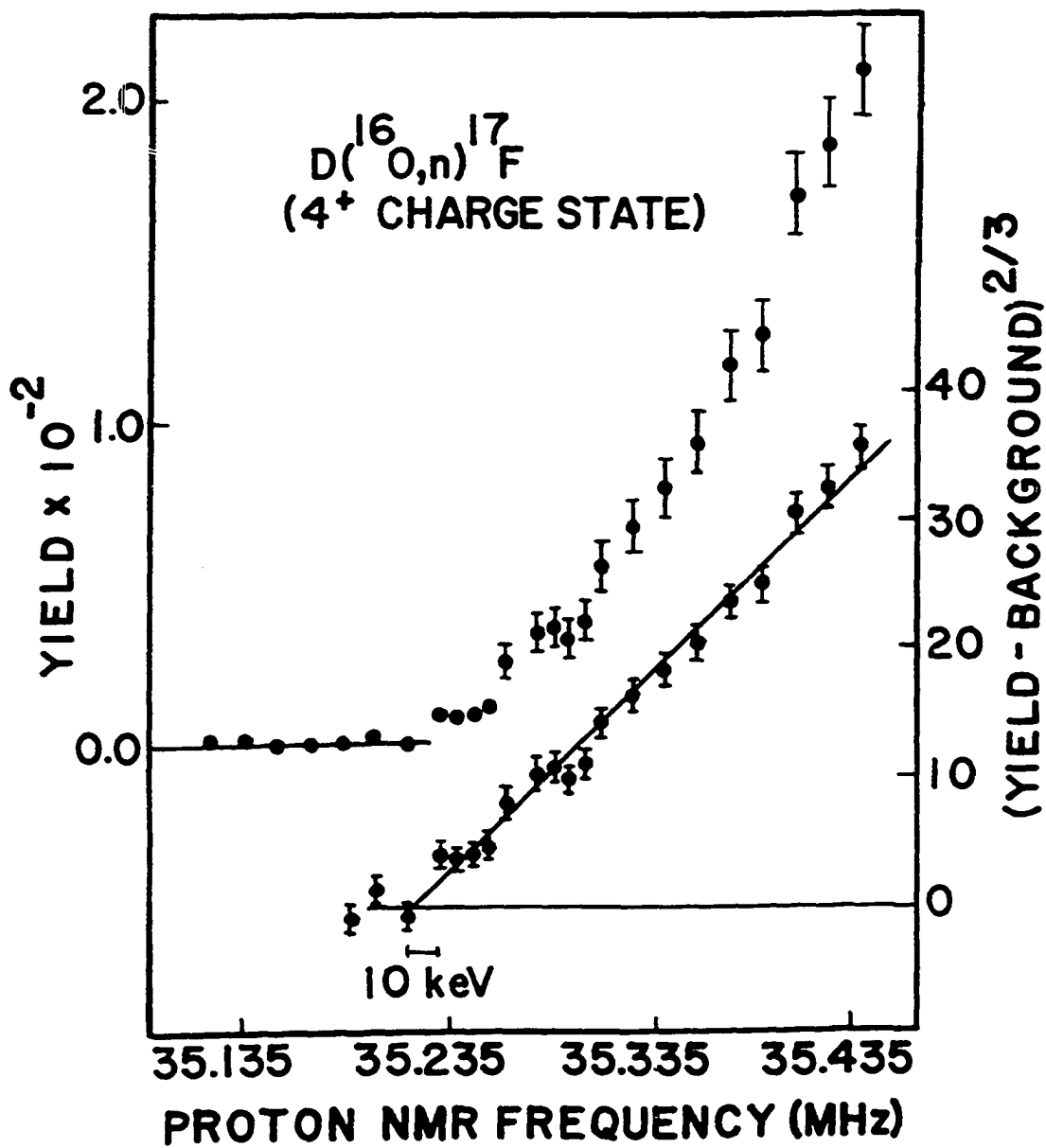


Figure IX. THRESHOLD MEASUREMENTS

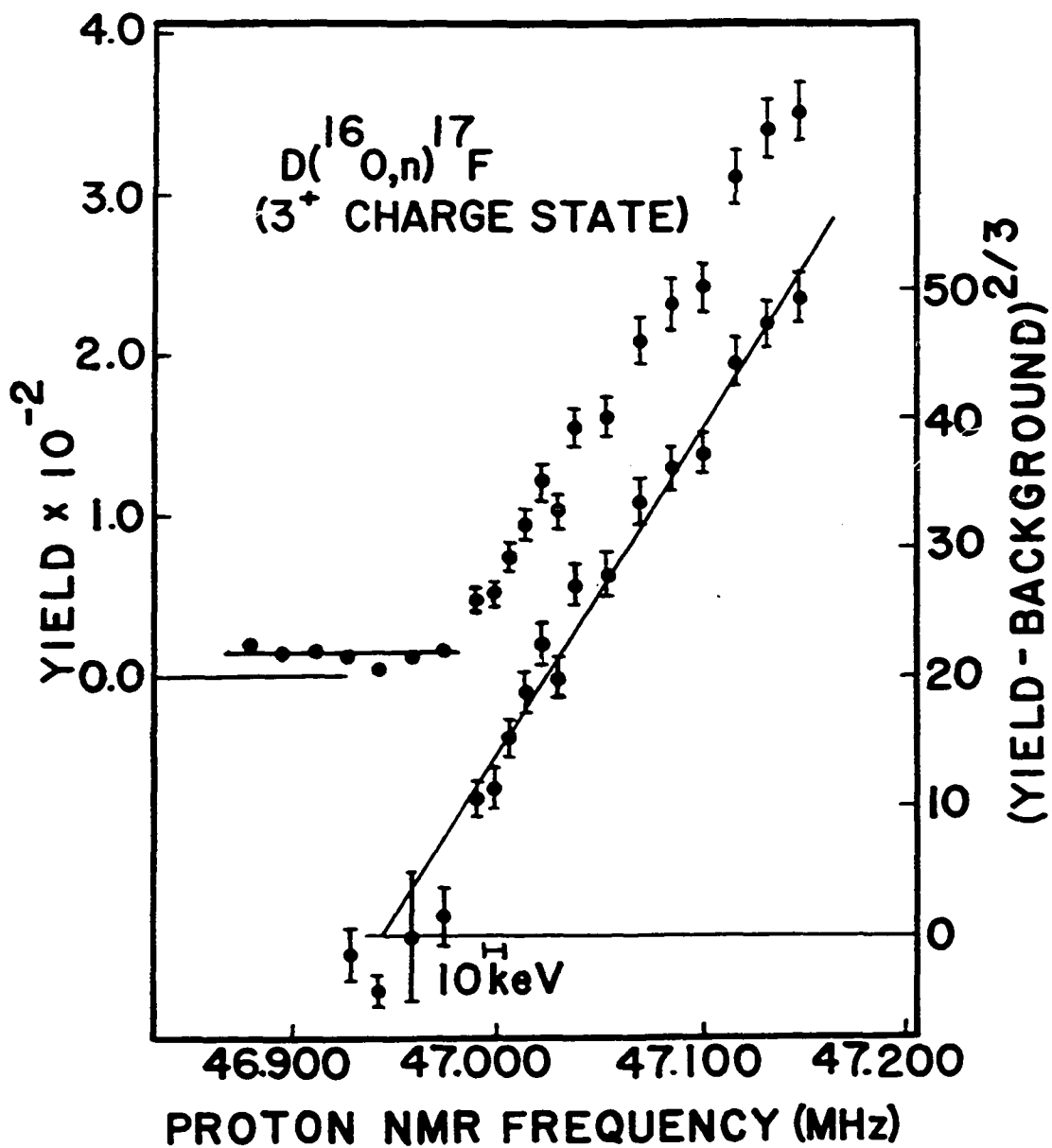


Figure X. THRESHOLD MEASUREMENTS

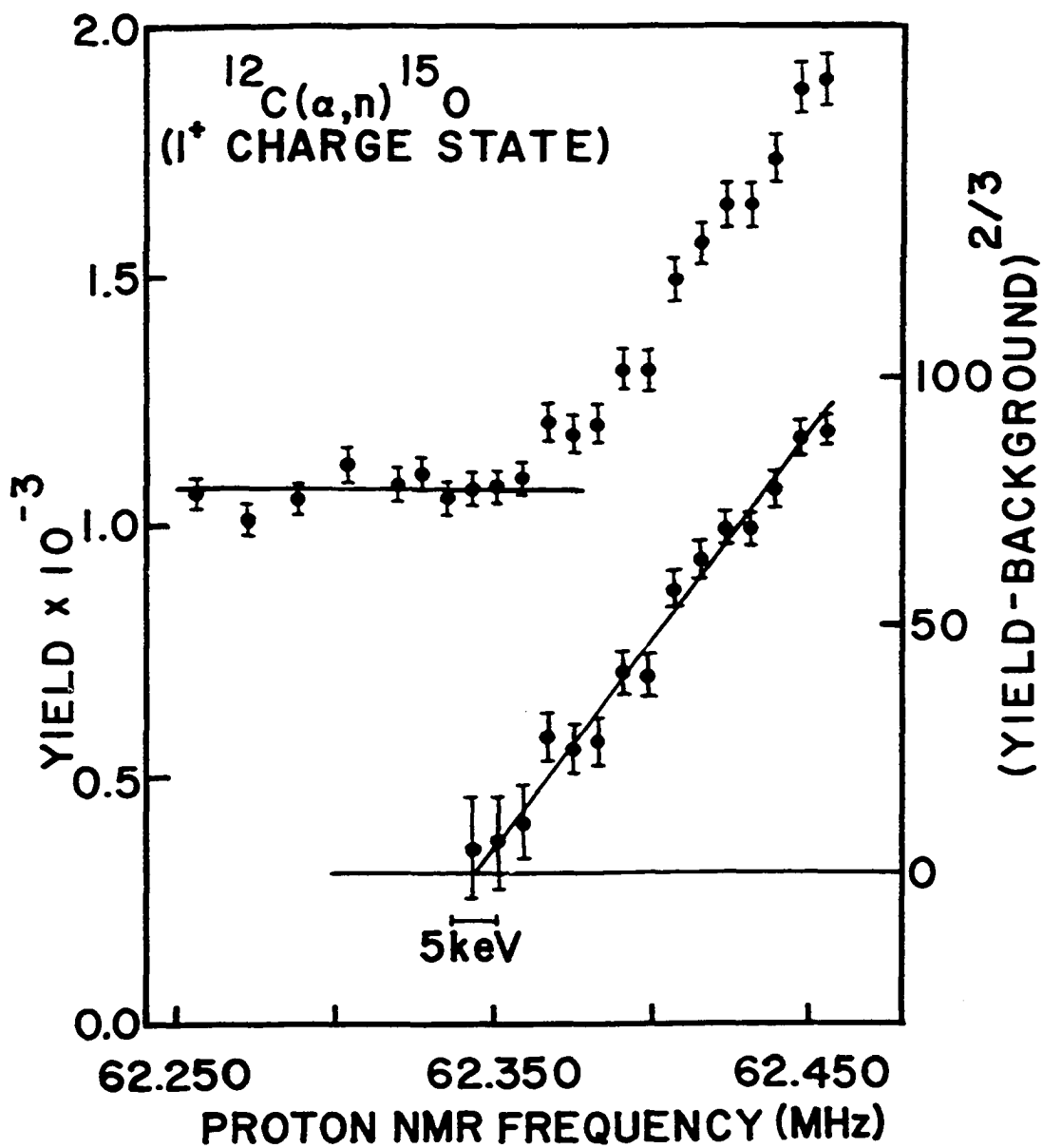


Figure XI. THRESHOLD MEASUREMENTS

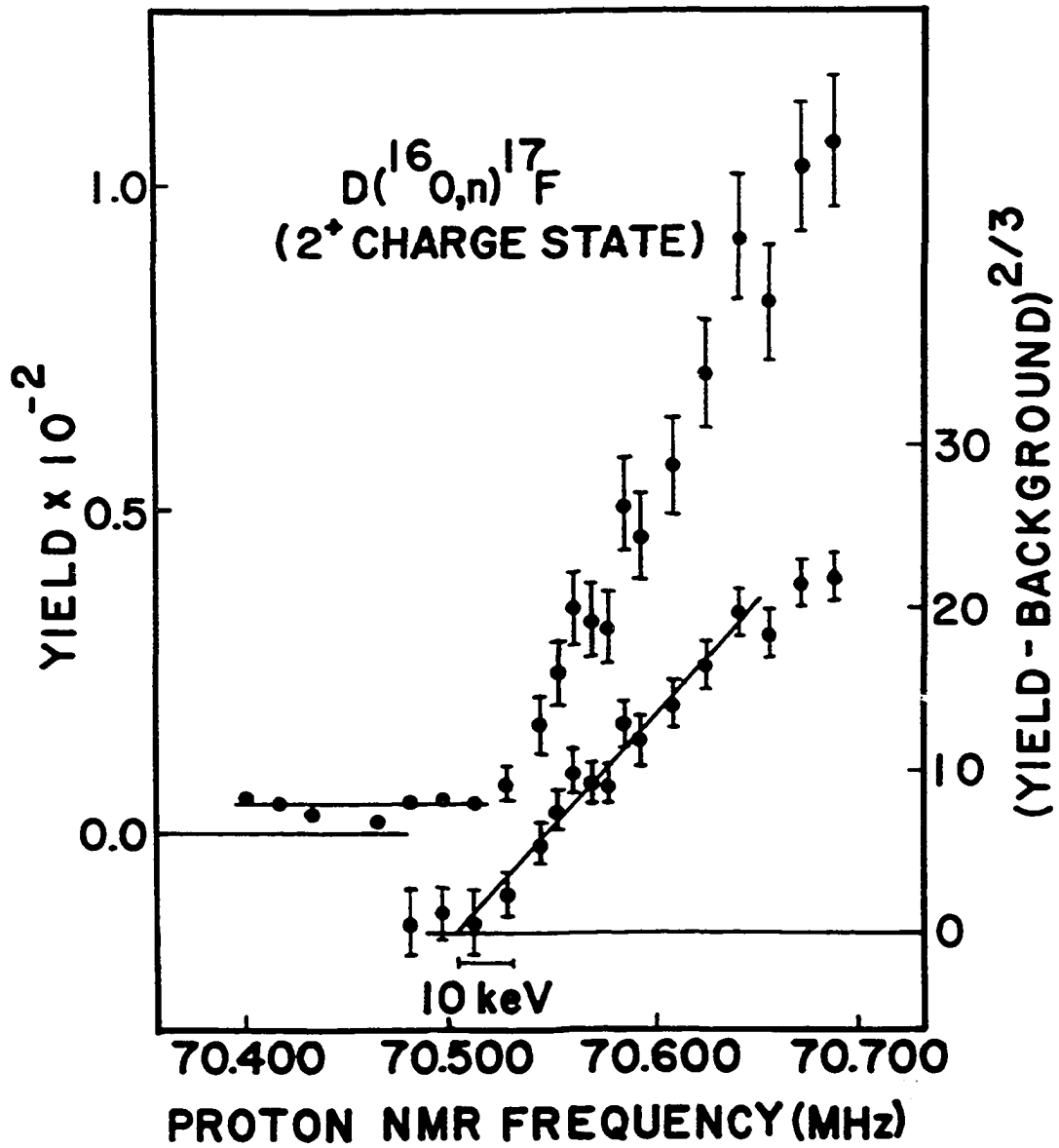


Figure XII. THRESHOLD MEASUREMENTS

Figure XIII. Magnet Constant Versus Proton NMR Frequency. The magnet constant, K , has been calculated for each of the nine threshold calibration points measured, and displayed on the plot at the appropriate proton NMR frequency. The shaded points represent the points used for the least squares straight line fit shown. At the ^{27}Al point, the shaded circle represents a K value calculated with the threshold energy of Freeman et al., while the open circle represents a K value calculated with the Bonner et al. threshold energy. At the ^{12}C points, the square points are K values calculated with a threshold energy which uses the Mattauch et al. ^{15}O mass, while the triangular points represent K values calculated using a threshold energy which uses Hensley's ^{15}O mass. For the purpose of the least squares fit, an average of these two masses, with an error encompassing the mass difference, was used to compute a threshold energy. This energy is used to calculate the K values at the ^{12}C points.

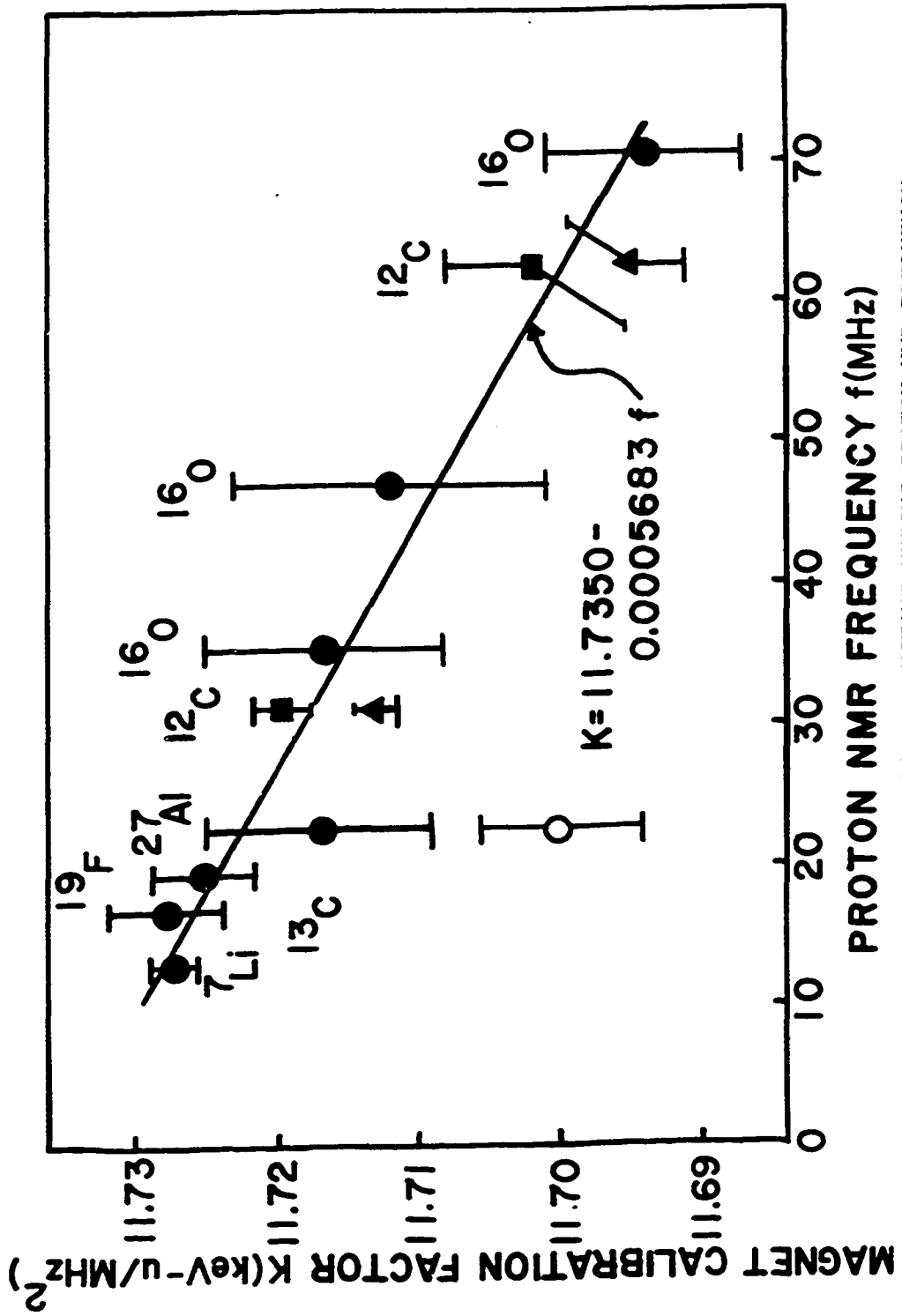


Figure XIII. MAGNET CONSTANT VERSUS PROTON NMR FREQUENCY

The threshold energies used in computing the value of the magnet constant from a given reaction threshold were, in most cases, those recommended and tabulated by Marion¹. The exceptions are the $^{27}\text{Al}(p,n)^{27}\text{Si}$ and $^{12}\text{C}(\alpha,n)^{15}\text{O}$ reactions.

The value of 5796.9 ± 3.8 keV for the $^{27}\text{Al}(p,n)^{27}\text{Si}$ threshold energy recommended by Marion represents the weighted average of two measurements, one by Freeman *et al.*¹⁴ of 5802.9 ± 3.8 keV and the other by Bonner *et al.*¹⁵ of 5794.5 ± 2.4 keV. It is seen that the value for the K computed using the Freeman value for the threshold energy (Shown as the closed circle at the ^{27}Al point on Fig. XIII.) is consistent with a line drawn through the points at other energies. However, the value of K computed using the Bonner energy value (Shown as the open circle at the ^{27}Al point on Fig. XIII.) lies more than three standard deviations from such a line. For this reason only the Freeman value for the threshold energy was used to calculate K for the $^{27}\text{Al}(p,n)^{27}\text{Si}$ reaction.

In the case of the $^{12}\text{C}(\alpha,n)^{15}\text{O}$ reaction the threshold energy recommended by Marion was calculated from the atomic masses given by Mattauch *et al.*¹⁶ However, a difference from the table of Mattauch of -4.6 ± 0.6 keV in the mass excess of ^{15}O has been reported recently by Hensley¹⁷. It appears that the Mattauch calculation of the ^{15}O mass is heavily weighted by a $^{15}\text{N}(p,n)^{15}\text{O}$ threshold energy measurement by Jones *et al.*¹⁸ In his measurement of the threshold, Jones employed the $^7\text{Li}(p,n)^7\text{Be}$ threshold, measured with H_2^+ ions bent 60° through his analyzing magnet, as a calibration reaction. Simultaneously, an H^+ beam was bent 90° through the magnet and the $^{15}\text{N}(p,n)^{15}\text{O}$

threshold was observed immediately after observing the calibration reaction. It appears that the incident beams for each of these reactions travel a different path through the magnet and thereby experience different magnetic fields. Thus, some doubt is cast upon the results of this $^{15}\text{N}(p,n)^{15}\text{O}$ threshold measurement, and hence, upon the Mattauch ^{15}O mass. The K value computed using each of the ^{15}O masses is consistent with values of K computed at other energies within the errors of the present experiment. Therefore, the average of these two values of the ^{15}O mass was used to calculate a threshold energy value and the mass discrepancy was included in the energy error. On Figure XIII at the ^{12}C points, the square points represent K values calculated with Marion's energy value, while the triangular points represent those calculated with a threshold energy using Hensley's ^{15}O mass.

The incident particle mass used, when calculating the value of the magnet constant for the proton induced reactions, was 1.00727663 u. For the alpha and ^{16}O induced reactions, the appropriate ionic mass, calculated by subtracting the correct number of electrons from the atomic mass, neglecting electron binding energies, was employed. In the case of the incident alpha particle 1^+ and 2^+ charge states, these masses were, respectively, 4.002055 and 4.001506 u. For the incident 2^+ , 3^+ , and 4^+ charge states of the ^{16}O ion, the masses were, respectively, 15.993818, 15.993269, and 15.992721 u.

The closed points in the plot on Figure XIII are the points used for the least squares straight line fit shown. At the ^{12}C points, as previously discussed, an average value of the two points with an

error encompassing both was used. The best fit straight line was:

$$K = \left(11.7350 \pm 0.0022 \frac{\mu\text{-keV}}{\text{MHz}^2} \right) - \left(0.0005683 \pm 0.000000118 \frac{\mu\text{-keV}}{\text{MHz}^2} \right) f \quad (23)$$

The errors shown on the figures and assigned to the results in Table I were determined in the standard manner as described, for example, by Bevington¹⁹. The error in the (yield-background)^{2/3} was calculated by the relation:

$$\left(\Delta(Y^{2/3}) / Y^{2/3} \right) = (2/3) (\Delta Y / Y), \quad (24)$$

where:

$$Y = \text{yield-background} = Y' - \bar{B},$$

$$\Delta Y = \text{error in } Y = \sqrt{(\Delta Y')^2 + (\Delta \bar{B})^2},$$

$$\Delta Y' = \text{error in yield} = \sqrt{Y'},$$

$$\Delta \bar{B} = \text{error in average background} = \sqrt{\sum_{i=1}^N B_i} / N,$$

$$B_i = \text{individual background point},$$

$$N = \text{total number of background points, and}$$

$$\Delta(Y^{2/3}) = \text{error in } Y^{2/3}.$$

The error in the threshold frequency result is the rms combination of the error in the average frequency and the standard deviation from run to run:

$$\Delta f = \sqrt{\left[\sum_{i=1}^M (\Delta f_i)^2 / M \right]^2 + \sigma_f^2}, \quad (25)$$

where:

$$\Delta f_i = \text{fit error (See Appendix I.)},$$

$$\sigma_f = \sqrt{\sum_{i=1}^M (f_i - \bar{f})^2 / (M-1)},$$

$$M = \text{number of individual threshold measurements,}$$

$$\bar{f} = \sum_{i=1}^M f_i / M = \text{threshold frequency result, and}$$

$$f_i = \text{individual threshold frequencies.}$$

The errors assigned to the magnet constants were calculated by com-

binning the uncertainty in the threshold frequency result, Δf , and the listed standard deviations in the energy values, ΔE :

$$\frac{\Delta K}{K} = \sqrt{\left(\frac{2\Delta f}{f}\right)^2 + \left(\frac{\Delta E}{E}\right)^2} \quad (26)$$

The major portion of the uncertainty in the magnet constant, in most cases, is due to the error in the energy values. The errors quoted for the constants in the straight line result of the K versus f plot, Eq. (23), were determined from the formulas derived by Bevington for a least squares weighted fit. The error in energies, calculated using Eq. (7), can be calculated using the errors determined for the constants in the linear K versus f plot, which are for $K=a+bf$, (a and b are the constants):

$$\Delta a = \text{error in } a = 0.0022 \text{ u-keV/MHz}^2, \text{ and}$$

$$\Delta b = \text{error in } b = 0.000000118 \text{ u-keV/MHz}^3.$$

Assuming $E \approx Kf^2$, then the error in the energy is:

$$\Delta E = \sqrt{(0.0022f^2)^2 + (0.000000118f^3)^2} \quad (27)$$

All data reduction leading to the results quoted was done on the Western Michigan University Computer Center's PDP 10 computer. The Fortran programs written for this purpose are listed in Appendix II. For the convenience of those operating the accelerator, a program was written for the PDP 15 computer, located in the accelerator control room, to print a table of frequencies and corresponding energies for various incident particles and charge states. A listing of this program is included in Appendix II.

SUMMARY AND CONCLUSIONS

The purpose of this thesis was to provide energy calibration for the Western Michigan University tandem accelerator. This was done by determining the magnet constant of the accelerator analyzing magnet for each of the nine neutron thresholds listed in Table I. These thresholds covered rather uniformly the full range of the field of the magnet, and thus, the full range of proton NMR frequency. The dependence of the magnet constant, K , upon the proton NMR frequency, f , was investigated, and it was found that the recycling procedure suggested by the magnet manufacturers, Varian, Associates, led to a simple straight line dependence of K upon f (See Fig. XIII and Eq. (23).). Using this K dependence result, the energy of any incident particle, with a given charge, and the energy error (See Eq. (27).) can be calculated in a straightforward manner from the NMR frequency by means of Eq. (7). It should be pointed out that the K dependence determined is only valid if the same recycling procedure as outlined in the Experimental section is employed.

In order to give some idea as to the accuracy of the accelerator calibration, the energy error was calculated for 2 MeV and 12 MeV incident protons. The calculated error for 2 MeV protons is 0.38 keV, whereas the error calculated for 12 MeV protons is 2.29 keV. It must be noted that this error represents the minimum estimate. Error due to reproducibility for a given measurement must also be included in the final error assignment.

In the course of interpreting the data to be used for the K versus f plot, there was ambiguity as to which threshold energies to use to calculate K values for the $^{27}\text{Al}(p,n)^{27}\text{Si}$ and $^{12}\text{C}(\alpha,n)^{15}\text{O}$ reactions. It is seen that, for the $^{27}\text{Al}(p,n)^{27}\text{Si}$ reaction, the Freeman energy value¹⁴ of 5802.9 ± 3.8 keV is the more consistent threshold energy, as opposed to the Bonner value¹⁵ of 5794.3 ± 2.4 keV, which lies more than three standard deviations from a curve drawn through K values at other energies (See Fig. XIII.). The threshold energy value of Marion represents a weighted average of these two, but previous work, by Overly et al.⁶ at Yale University, as well as this work, favors the Freeman value. It would seem that another measurement of this reaction's threshold energy would be of value. In the case of the $^{12}\text{C}(\alpha,n)^{15}\text{O}$ reaction, the threshold energy recommended by Marion is calculated from the masses involved. Recently Hensley¹⁷ has reported a mass for ^{15}O which is lower than that tabulated by Mattauch et al.¹⁶ by 4.6 ± 0.6 keV (See Results and Discussion section.). K values calculated with threshold energies determined with each ^{15}O mass are consistent with data at other energies (See Fig. XIII.), and thus, the average value with an error encompassing the mass discrepancy was used. It is pointed out that a remeasurement of the $^{15}\text{N}(p,n)^{15}\text{O}$ threshold energy to investigate the validity of the Jones et al.¹⁸ measurement (See Results and Discussion section.) might prove valuable in determining the correct ^{15}O mass.

This work is believed to represent the first attempt to calibrate an accelerator by directly observing neutrons from the $^{12}\text{C}(\alpha,n)^{15}\text{O}$ reaction. It is noted that, even with the ^{15}O mass discrepancy in-

cluded (See Results and Discussion section and Fig. XIII.), these points are at least as good as the $D(^{16}\text{O},n)^{19}\text{F}$ reaction points for calibration purposes. The $^{12}\text{C}(\alpha,n)^{15}\text{O}$ reaction is advantageous in that solid ^{12}C targets are easily obtainable and one does not need to employ an elaborate target assembly as in the case of ice targets. It is a fact also that alpha particle beams are becoming common, so that this reaction can be easily employed. Further investigation of the ^{15}O mass, i.e., by a measurement of the $^{15}\text{N}(p,n)^{15}\text{O}$ threshold, will significantly increase the precision and value of the $^{12}\text{C}(\alpha,n)^{15}\text{O}$ reaction points as high energy calibration points.

Finally, the investigation in this work of the possibility of employing the $^{16}\text{O}(\alpha,n)^{19}\text{Ne}$ reaction for high field calibration points suggests that this reaction threshold does not provide calibration points which are easily observable with a long counter.

APPENDIX I

The best straight line through a set of data points,

$$y_i = a + b x_i \quad (1)$$

where x_i is (net yield)^{2/3}, y_i is NMR frequency, and a and b are constants, can be determined via the method of least squares. If the uncertainty is in the x_i , then the weighted sum of the square of the x residuals²⁰,

$$S = \sum_i w_i (\text{res})^2$$

or
$$S = \sum_i w_i [x_i - (y_i - a)/b]^2, \quad (2)$$

where the weighting, w_i , is $1/(\Delta x_i)^2$, and Δx_i is the uncertainty in x_i , must be minimized. This is done by setting the appropriate partial derivatives equal to zero,

$$\partial S / \partial a = 2/b \sum_i w_i (x_i - y_i/b + a/b) = 0 \quad (3)$$

and
$$\partial S / \partial b = 2/b^2 \sum_i w_i (y_i - a)(x_i - y_i/b + a/b) = 0 \quad (4)$$

These two derivatives yield:

$$b \sum_i w_i x_i + a \sum_i w_i - \sum_i w_i y_i = 0 \quad (5)$$

and
$$b \sum_i w_i x_i y_i - ab \sum_i w_i x_i + 2a \sum_i w_i y_i - a^2 \sum_i w_i - \sum_i w_i y_i^2 = 0, \quad (6)$$

Solving for b in Eq. (5) and substituting into Eq. (6), one gets

for a:

$$a = \frac{\sum_i w_i y_i^2 \sum_i w_i x_i - \sum_i w_i y_i \sum_i w_i x_i y_i}{\sum_i w_i y_i \sum_i w_i x_i - \sum_i w_i \sum_i w_i x_i y_i} \quad (7)$$

Using this value for a, b may be calculated from Eq. (5):

$$b = \frac{\sum_i w_i y_i - a \sum_i w_i}{\sum_i w_i x_i} \quad (8)$$

The value of a, in this case, is the value of the threshold frequency, f.

To derive the fit error, ΔF_i , which is the standard deviation in a , σ_a , one uses the relation:

$$\sigma_a^2 = \sum_j [\Delta x_j^2 \left(\frac{\partial a}{\partial x_j} \right)^2]. \quad (9)$$

It is first necessary to calculate $\frac{\partial a}{\partial x_j}$

$$\frac{\partial a}{\partial x_j} = \frac{\partial}{\partial x_j} \left\{ \frac{\sum_i w_i y_i^2 \sum_i w_i x_i - \sum_i w_i y_i \sum_i w_i x_i y_i}{\sum_i w_i y_i \sum_i w_i x_i - \sum_i w_i \sum_i w_i x_i y_i} \right\}$$

or

$$\frac{\partial a}{\partial x_j} = \frac{1}{\text{denomin.}} [w_j \sum_i w_i y_i^2 - w_j y_j \sum_i w_i y_i] + \frac{\text{numerator}}{(\text{denominator})^2} (-1) [w_j \sum_i w_i y_i - w_j y_j \sum_i w_i]$$

Noting that numerator/denominator is a and gathering terms one gets:

$$\frac{\partial a}{\partial x_j} = \frac{1}{\text{denominator}} \left[w_j \left(\sum_i w_i y_i^2 - a \sum_i w_i y_i \right) - w_j y_j \left(\sum_i w_i y_i - a \sum_i w_i \right) \right]$$

Letting

$$Q = \sum_i w_i y_i^2 - a \sum_i w_i y_i$$

and

$$R = \sum_i w_i y_i - a \sum_i w_i$$

one obtains:

$$\left(\frac{\partial a}{\partial x_j} \right)^2 = \frac{1}{(\text{denomin.})^2} \left[w_j^2 Q^2 + w_j^2 y_j^2 R^2 - 2 w_j^2 y_j Q R \right]. \quad (10)$$

Thus, from Eq. (9),

$$\sigma_a^2 = \frac{1}{(\text{denomin.})^2} \sum_j \left\{ \Delta x_j^2 w_j^2 Q^2 + \Delta x_j^2 w_j^2 y_j^2 R^2 - 2 \Delta x_j^2 w_j^2 y_j Q R \right\}, \quad (11)$$

or

$$\sigma_a^2 = \frac{1}{(\text{denomin.})^2} \left[Q^2 \sum_j w_j + R^2 \sum_j w_j y_j^2 - 2 Q R \sum_j w_j y_j \right] \quad (12)$$

since

$$\Delta x_j^2 w_j^2 = w_j.$$

APPENDIX II

This section contains a listing of four Fortran programs written to handle the data taken in this experiment. The first three programs are designed for execution on Western Michigan Computer Center's PDP 10 computer. The last program was written specifically for the PDP 15 computer located in the accelerator control room.

The first program is entitled THRESH.F4. Its purpose is to determine the threshold frequency and frequency error, through a least squares straight line extrapolated fit (See Appendix I.) of frequency versus (yield-background)^{2/3}. The second program, entitled KVAL.F4, calculates the magnet constant and its error for a given threshold reaction. The third program is entitled POLY.F4 and its function is to perform a standard least squares fit to data with error in the y coordinate. It was written specifically to determine the fit polynomial of the K versus f plot illustrated in Fig. XIII. The fit can be a first, second, or third order polynomial. In the case when a first order (straight line) fit is warranted, as was the case for the K versus f plot, the error in the two constants is computed. The fourth program, entitled ENERGY, calculates the energies of various incident particles and charge states from frequencies and prints them in tabular form. The main variables for the programs are listed in the comment lines preceding each program.

```

C      THRESH,F4
C      THIS IS A PROGRAM TO ANALYZE THRESHOLD DATA
C      THE MAIN VARIABLES ARE AS FOLLOWS:
C          M: TOTAL NOS. OF PTS.
C          N: NOS. OF BACKGROUND PTS.
C          L: NOS. OF FIT PTS.
C          LB: NOS. OF PTS AT THE START OF ARRAY NOT USED
C          X(I): FREQUENCY
C          Y(I): NEUTRON YIELD
C          B: BACKGROUND BELOW THRESHOLD
C          YS(I): NET YIELD ABOVE BACKGROUND = Y(I)-B
C          Z(I): NET YIELD TO THE 2/3 POWER
C          DB: ERROR IN B
C          DYS(I): ERROR IN YS(I)
C          DZ(I): ERROR IN Z(I)
C          A: INTERCEPT OF  $X = A + BA^Y$  FIT OR THRESHOLD FREQUENCY
C          BA: SLOPE OF  $X = A + BA^Y$  FIT
C          SA: THRESHOLD FREQUENCY ERROR
C          DOUBLE PRECISION SUM,XSUM,YSUM,QSUM,DSUM,ASUM,X2SUM
C          DOUBLE PRECISION Z,DZ,C,DELTA,BA,A,SB,Q,DYS,YS,X,Y,B,DB,R
C          DIMENSION X(35),Y(35),DY(35),YS(35),DYS(35),Z(35),DZ(35)
1      READ (5,100) M
C          TYPE 99,M
99      FORMAT (' TOTAL NOS. OF PTS. IS ',I2/)
100     FORMAT(I2)
C          TYPE 98
98      FORMAT (' I',5X,' X',8X,' Y'/)
C          DO 6 I=1,M
C          READ (5,110) X(I),Y(I)
6          TYPE 97,I,X(I),Y(I)
97      FORMAT (I3,1X,F9.4,F9.0)
110     FORMAT (2F).
2          TYPE 101
101     FORMAT (' TYPE NOS. OF BACKGROUND PTS.'/)
C          ASUM=0.
C          ACCEPT 100,N
C          IF (N.EQ.0) CALL EXIT
C          DO 20 I=1,N
20      ASUM=ASUM+Y(I)
C          TN=N
C          B=ASUM/TN
C          DB=DSQRT(ASUM)/TN
23      TYPE 111
111     FORMAT (' TYPE NOS. OF PTS. AT START OF ARRAY NOT USED'/)
C          ACCEPT 100, LB
C          IF (LB.EQ.0) GO TO 2
25      TYPE 112
112     FORMAT (' TYPE NOS. OF TOTAL PTS. USED'/)
C          ACCEPT 100, L
C          IF (L.EQ.0) GO TO 23

```

```

DO 30 J=1,L
K=LB+J
YS(J)=Y(K)-B
DYS(J)=DSQRT(Y(K)+DB DB)
Z(J)=(YS(J)*YS(J))**(1./3.)
30 DZ(J)=(2.*DYS(J)*Z(J))/(3.*YS(J))
TYPE 113
113 FORMAT (' FIT PTS. PRINTED? YES=CAR. RET., NO=01'/)
ACCEPT 100, NOS
IF (NOS.EQ.1) GO TO 40
TYPE 114
114 FORMAT (' I',4X,' X(I)',6X,' Y 2/3',6X,' DY 2/3'/)
DO 45 I=1,L
KI=LB+I
TYPE 115, I, X(KI), Z(I), DZ(I)
115 FORMAT (I3,3X,F7.4,4X,F8.3,5X,F8.4)
45 CONTINUE
C
C LEAST SQUARES FIT
C
40 XSUM=0.
YSUM=0.
X2SUM=0.
DSUM=0.
SUM=0.
QSUM=0.
TL=L
DO 9 I=1,L
C=DZ(I) DZ(I)
MI=LB+I
XSUM=XSUM+X(MI)/C
DSUM=DSUM+(1./C)
YSUM= YSUM+(Z(I)/C)
SUM=SUM+(X(I)*Z(I))/C
X2SUM=X2SUM+X(MI)*X(MI)
9 QSUM=QSUM+(Z(I)*Z(I))/C
DELTA= XSUM YSUM-DSUM*SUM
A=(X2SUM*YSUM-XSUM*SUM)/DELTA
BA= (XSUM-A*DSUM)/YSUM
R=XSUM-A*DSUM
Q=X2SUM-A*XSUM
IF (DELTA) 11,12,12
11 DELTA=(-1)*DELTA
12 CONTINUE
SA=(DSQRT(Q*Q*DSUM+R*R*X2SUM-2.*Q*R*XSUM)/DELTA)
TYPE 102
102 FORMAT (' FREQUENCY=A+B*(YIELD-BACKGROUND)*2/3'/)
TYPE 103,A,BA
103 FORMAT (' A = ',E15.9,' B = ',E15.9/)
TYPE 104,A
104 FORMAT (' THRESHOLD = ',F11.7/)

```

```

TYPE 106, SA
106  FORMAT (' ERROR IN THE THRESHOLD IS ',F11.8/)
      GO TO 25
      END

C     KVAL.F4
C     THIS IS A PROGRAM TO COMPUTE THE MAGNET CALIBRATION
C     CONSTANT, K, FOR VARIOUS THRESHOLD REACTIONS.
C     THE MAIN VARIABLES ARE AS FOLLOWS:
C       K: MAGNET CALIBRATION CONSTANT
C       DK: ERROR IN THE MAGNET CALIBRATION CONSTANT
C       E: THRESHOLD ENERGY
C       DE: ERROR IN THE THRESHOLD ENERGY
C       Q: CHARGE OF THE INCIDENT PARTICLE
C       F: THRESHOLD FREQUENCY
C       DF: ERROR IN THE THRESHOLD FREQUENCY
      REAL K
1     TYPE 100
100   FORMAT (' TYPE THE THRESHOLD ENERGY AND ITS ERROR IN KEV'/)
      ACCEPT 101, E, DE
101   FORMAT (2F)
      IF (E.EQ.0.) CALL EXIT
20    TYPE 102
102   FORMAT (' TYPE THE CHARGE OF THE INCIDENT PARTICLE IN DECIMAL
1     FORM'/)
      ACCEPT 101, Q
      IF (Q.EQ.0.) GO TO 1
      TYPE 103
103   FORMAT (' TYPE THE MASS OF THE INCIDENT PARTICLE IN U'/)
      ACCEPT 101, A
30    TYPE 104
104   FORMAT (' TYPE THE THRESHOLD FREQUENCY AND ERROR IN MHZ'/)
      ACCEPT 101, F, DF
      IF (F.EQ.0.) GO TO 20
      C=((A*1.660436*(299792500.))**2.)/1.6021/100000000000.
      B=E/(2.*C)
      K=((A*E)/(Q*Q*F*F))*(1.+B)
      DK=K SQRT(4.*(DF/F)**2.+(DE/E)**2.)
      TYPE 105, K, DK
105   FORMAT (' K = ',F15.8,' + OR - ',F15.8)
      GO TO 30
      END

C     POLY.F4
C     THIS IS A PROGRAM TO FIT A POLYNOMIAL OF ORDER THREE
C     OR LESS TO A SET OF DATA POINTS OF THE FORM (X(I),
C     Y(I) + OR - DY(I)), FOR I LESS THAN OR EQUAL TO 35,
C     BY THE METHOD OF LEAST SQUARES.
C
C     THE MAIN VARIABLES ARE AS FOLLOWS:

```

```

C      N: NOS. OF TOTAL PTS.
C      X(I): X VALUE
C      Y(I): Y VALUE
C      DY(I): ERROR IN THE Y VALUE
C      NO: ORDER OF THE POLYNOMIAL FIT
C      A(I): CONSTANTS OF THE POLYNOMIAL  $Y=A(1)+A(2)X+A(3)X^{**2}+$ 
C            $A(4)X^{**3}$ 
C      SA1: ERROR IN A(1), IF FIRST ORDER FIT
C      SA2: ERROR IN A(2), IF FIRST ORDER FIT
DIMENSION X(35),Y(35),DY(35),Z(4,5),SUM(15),TEMP(4),A(4)
COMMON Z
1     TYPE 90
90    FORMAT (' I',4X,' X',10X,' Y',10X,' DY'/)
      READ (5,101) N
101   FORMAT (I2)
      IF (N.EQ.0) CALL EXIT
      DO 26 I=1,N
      READ (5,103) X(I),Y(I),DY(I)
103   FORMAT (2F)
26    TYPE 102, I, X(I), Y(I), DY(I)
102   FORMAT (I3,3F11.7)
5     TYPE 108
108   FORMAT (' TYPE ORDER OF FIT POLYNOMIAL'/)
      ACCEPT 101, NO
      IF (NO.EQ.0) GO TO 1
      DO 30 I=1,15
30    SUM(I)=0.
      DO 35 I=1,N
      Q=DY(I) 2.
      SUM(1)=SUM(1)+1./Q
      SUM(2)=SUM(2)+X(I)/Q
      SUM(3)=SUM(3)+X(I)**2./Q
      SUM(4)=SUM(4)+X(I)**3./Q
      SUM(5)=SUM(5)+X(I)**4./Q
      SUM(6)=SUM(6)+X(I)**5./Q
      SUM(7)=SUM(7)+X(I)**6./Q
      SUM(8)=SUM(8)+Y(I)/Q
      SUM(9)=SUM(9)+(X(I)*Y(I))/Q
      SUM(10)=SUM(10)+(X(I)**2.*Y(I))/Q
      SUM(11)=SUM(11)+(X(I)**3.*Y(I))/Q
35    CONTINUE
      DO 40 I=1,4
      Z(1,I)=SUM(I)
      IF (I.EQ.4) GO TO 40
      Z(I+1,4)=SUM(I+4)
40    Z(I,5)=SUM(I+7)
      Z(2,3)=Z(1,4)
      Z(3,3)=Z(2,4)
      Z(2,2)=Z(1,3)
      DO 45 I=1,3
      DO 50 J=2,4

```

```

50     Z(J,I)=Z(I,J)
45     CONTINUE
      IF (NO.EQ.1) GO TO 61
      CALL DET2(Z(1,1),Z(1,2),Z(2,1),Z(2,2),ANS1)
      GO TO 53
C     CRAMER'S RULE TO SOLVE FOR A(I)'S
61     IF (NO.EQ.2) GO TO 52
      CALL DET4(ANS1)
      IF (NO.EQ.3) GO TO 53
52     CALL DET3(ANS1)
53     DO 60 I=1,NO+1
      DO 70 J=1,NO+1
      TEMP(J)=Z(J,I)
70     Z(J,I)=Z(J,5)
      IF (NO.EQ.1) GO TO 66
      CALL DET2(Z(1,1),Z(1,2),Z(2,1),Z(2,2),ANS2)
      GO TO 64
66     IF (NO.EQ.2) GO TO 63
      CALL DET4(ANS2)
      IF (NO.EQ.3) GO TO 64
63     CALL DET3(ANS2)
64     DO 65 K=1,NO+1
65     Z(K,I)=TEMP(K)
60     A(I)=ANS2/ANS1
      DO 69 J=1,NO+1
69     TYPE 105, J, A(J)
105    FORMAT (' A( ',I2,' ) = ',E15.7/)
      IF (NO.NE.1) GO TO 5
      CONST=SUM(3)*SUM(1)-SUM(2)**2.
      SA2=SQRT(1./CONST)
      SA1=SQRT(SUM(3)/CONST)
      TYPE 120, SA1, SA2
120   FORMAT (' ERROR IN A(1) =',E15.9,' ERROR IN A(2) =',E15.9/)
      GO TO 5
      END

C
C     SUBROUTINE TO CALCULATE A 2BY2 DETERMINATE
C
      SUBROUTINE DET2(A1,A2,A3,A4,A5)
      A5=A1*A4-A2*A3
      RETURN
      END

C
C     SUBROUTINE TO CALCULATE A 3BY3 DETERMINATE
C
      SUBROUTINE DET3(VAL3)
      COMMON Z
      DIMENSION Z(4,5),D(3)
      DO 16 I=1,2
16     CALL DET2(Z(2,I),Z(2,3),Z(3,I),Z(3,3),D(I))
      CALL DET2(Z(2,1),Z(2,2),Z(3,1),Z(3,2),D(3))

```

```

VAL3=Z(1,1)*D(2)-D(1)*Z(1,2)+Z(1,3)*D(3)
RETURN
END

C
C   SUBROUTINE TO CALCULATE A 4BY4 DETERMINATE
C
SUBROUTINE DET4(VAL)
COMMON Z
DIMENSION Z(4,5),B(12),C(6)
J=0
DO 11 I=1,4
DO 10 I=1,4
IF (K.EQ.1) GO TO 10
J=J+1
B(J)=Z(1,I)*Z(2,K)
10 CONTINUE
11 CONTINUE
DO 15 I=1,3
CALL DET2(Z(3,I),Z(3,4),Z(4,I),Z(4,4),C(I))
15 CONTINUE
CALL DET2(Z(3,2),Z(3,3),Z(4,2),Z(4,3),C(4))
DO 20 J=2,3
20 CALL DET2(Z(3,1),Z(3,J),Z(4,1),Z(4,J),C(J+3))
VAL=B(1)*C(3)-B(2)*C(2)+B(3)*C(4)-B(4)*C(3)+B(5)*C(1)-B(6)*
1 C(6)+B(7)*C(2)-B(8)*C(1)+B(9)*C(5)-B(10)*C(4)+B(11)*C(6)-
2 B(12)*C(5)
RETURN
END

C   THIS IS A PROGRAM TO GET PARTICLE ENERGIES FROM PROTON NMR
C   FREQUENCIES AND THEN TO PRODUCE A TABLE OF FREQUENCIES AND
C   ENERGIES.
C   THE MAIN VARIABLES ARE AS FOLLOWS:
C       XM: MASS OF THE INCIDENT PARTICLE
C       Q: CHARGE OF THE INCIDENT PARTICLE
C       F: PROGRAM STARTING FREQUENCY
C       T: SWITCH FOR F/8, F/4, OR F/2 CHOICE
C       DDDF: INCREMENT FOR CHOICE
C       ES: STARTING ENERGY FOR TABLE
C       EF: ENDING ENERGY FOR TABLE
C       FV: FREQUENCY USED IN CALCULATIONS
C       DFF: INCREMENT FOR FV
C       VK: MAGNET CONSTANT
C       E(I): PARTICLE ENERGIES
C       IE(I): PARTICLE ENERGIES PRINTED, ROUNDED TO NEAREST KEV
C       FF: F/8, F/4, F/2 (DEPENDING ON CHOICE)
C       DDF: INCREMENT FOR FF
C
DOUBLE PRECISION B, C, DSQRT
DIMENSION E(10),IE(10),DF(10),DDF(10)
COMMON FV

```

```

1      WRITE (4,100)
100    FORMAT (44H TYPE MASS OF INCIDENT PARTICLE IN U.(F10.8)/)
      READ (4,200) XM
200    FORMAT (10.8)
3      WRITE (4,101)
101    FORMAT (41H TYPE CHARGE OF INCIDENT PARTICLE.(F10.8)/)
      READ (4,200) Q
5      WRITE (4,102)
102    FORMAT (39H TYPE STARTING FREQUENCY IN MHZ.(F10.8)/)
      READ (4,200) F
      IF (F.EQ.0) GO TO 1
6      WRITE (4,90)
90     FORMAT (30H F/8 = 1., F/4 = -1., F/2 = 0./)
      READ (4,200) T
      WRITE (4,112)
112    FORMAT (49H TYPE FREQUENCY INCREMENT FOR THIS CHOICE.(F10.8)/)
      READ (4,200) DDDF
7      WRITE (4,103)
103    FORMAT (36H TYPE STARTING ENERGY IN KEV.(F10.8)/)
      READ (4,200) ES
9      WRITE (4,104)
104    FORMAT (34H TYPE ENDING ENERGY IN KEV.(F10.8)/)
      READ (4,200) EF
      S=0.
      K=10
      J=1
      FV=F
      IF (T) 300,301,302
300    DFF=DDDF*4.
      GO TO 11
301    DFF=DDDF*2.
      GO TO 11
302    DFF=DDDF*8.
C
C      CALCULATION OF E(I)'S
C
11     CALL SUB1(VK)
      B=XM*931481.101
      C=(-1.)*VK*B*(Q**2.)*(FV**2.)/XM
      E(J)=((-1.)*B+DSQRT(B*B-2.*C))
      IF (E(J).LE.ES) GO TO 15
      S=1.
      IF (E(J).LE.EF) GO TO 15
      IF (J.EQ.10) GO TO 30
15     FV=FV+DFF
      J=J+1
      IF (J.LE.10) GO TO 11
      IF (S.EQ. 1.) GO TO 30
      J=1
      F=FV
      GO TO 11

```

```

30   IF (K.NE.10) GO TO 61
C
C   PRINTING OF HEADINGS
C
      DF(1)=0.
      DO 32 I=2,10
      L=I-1
32   DF(I)=DF(L)+DFF
      WRITE (4,105) (DF(I),I=1,10)
105  FORMAT ( 8X,2H F,3X,10F6.3)
      DDF(1)=0.
      DO 35 I=2,10
      M=I-1
34   DDF(I)=DDF(M)+DDDF
35   CONTINUE
      IF (T) 310,311,312
311  CONTINUE
      WRITE (4,106) (DDF(I),I=1,10)
106  FORMAT ( 7X,4H F/2,2X,10F6.3)
      WRITE (4,107)
107  FORMAT ( 2X,2H F,3X,4H F/2)
      GO TO 60
310  CONTINUE
      WRITE (4,108) (DDF(I),I=1,10)
108  FORMAT ( 7X,4H F/4,2X,10F6.3)
      WRITE (4,109)
109  FORMAT ( 2X,2H F,3X,4H F/4)
      GO TO 60
312  CONTINUE
      WRITE (4,110) (DDF(I),I=1,10)
110  FORMAT ( 7X,4H F/8,2X,10F6.3)
      WRITE (4,111)
111  FORMAT ( 2X,2H F,3X,4H F/8)
60   K=0
61   DO 75 I=1,10
75   IE(I)=E(I)+.5
C
C   PRINTING OF TABLE
C
      IF (T) 71,70,72
70   FF=F/2.
      GO TO 80
71   FF=F/4.
      GO TO 80
72   FF=F/8.
80   WRITE (4,113) F,FF,(IE(I),I=1,10)
113  FORMAT ( F6.2,1X,F5.3,1X,10I6)
      IF (E(10).GT.EF) GO TO 5
      K=K+1
      J=1
      F=FV

```

```
GO TO 11
END
C
C   SUBROUTINE TO CALCULATE THE MAGNET CONSTANT
C
SUBROUTINE SUB1(VAL)
COMMON FV
VAL=11.73496-.0005683*FV
RETURN
END
```

BIBLIOGRAPHY

1. J.B. Marion, Rev. Mod. Phys. 38, 660 (1966).
2. H.E. Gove, J.A. Kuehner, A.E. Litherland, E. Almqvist, D.A. Bromley, A.J. Ferguson, P.H. Rose, R.P. Bastide, N. Brooks, and R.J. Conner, Phys. Rev. Letters 1, 251 (1958).
3. R.O. Bondelid, J.W. Butler, and C.A. Kennedy, Phys. Rev. 120, 889 (1960).
4. J.W. Nelson, E.B. Carter, G.E. Mitchell, R.H. Davis, Phys. Rev. 129, 1723 (1963).
5. J.L. Black, H.M. Kuan, W. Gruhle, M. Suffert, and G.L. Latshaw, Nucl. Phys. A115, 687 (1968).
6. J.C. Overly, P.D. Parker, and D.A. Bromley, Nucl. Instr. and Meth. 68, 61 (1969).
7. J.D. Jackson, Classical Electrodynamics, John Wiley & Sons, Inc., New York, 1962, p. 411.
8. J.B. Marion, T.W. Bonner, Fast Neutron Physics, J.B. Marion and J.L. Fowler, ed., Interscience Publishers, Inc., New York, 1963, Part II, p. 1865.
9. E. Merzbacher, Quantum Mechanics, John Wiley & Sons, Inc., New York, 1970, Second Edition, p. 479.
10. E. Fermi, Nuclear Physics, J. Orear, A.H. Rosenfeld, and R.A. Shluter, ed., University of Chicago Press, 1949, Revised Edition, p.141.
11. R.D. Evans, The Atomic Nucleus, McGraw-Hill, New York, 1955, p. 637.
12. A.O. Hanson, R.F. Tascheck, and J.H. Williams, Revs. Modern Phys. 21, 635 (1949).
13. A.O. Hanson, and J.L. McKibben, Phys. Rev. 72, 673 (1947).
14. J.M. Freeman, J.H. Montague, G. Murray, R.E. White, and W.E. Burcham, Nucl. Phys. 65, 113 (1965).
15. B.E. Bonner, G. Rickards, D.L. Bernard, and G.C. Philips, Nucl. Phys. 86, 187 (1966).

16. J.H.E. Mattauch, W. Theile, and A.H. Wapstra, Nucl. Phys. 67, 1 (1965).
17. D.C. Hensley, Ph.D. Thesis, California Institute of Technology, 1969.
18. K.W. Jones, L.J. Lidofsky, and J.L. Wiel, Phys. Rev. 112, 1252 (1958).
19. P.R. Bevington, Data Reduction and Error Analysis for the Physical Sciences, McGraw-Hill, New York, 1969.
20. W. Edwards Deming, Statistical Adjustment of Data, Dover Publications, Inc., New York, 1964, p. 14.